MPK12 in stomatal CO_2 signaling: function beyond its kinase activity

Chung-Yueh Yeh*[1], Yuh-Shuh Wang*[1], Yohei Takahashi[2], Katarina Kuusk[1], Karnelia Paul[3], Triinu Arjus[1], Oleksii Yadlos[1], Julian I. Schroeder[3], Ivar Ilves[1], Alfonso T. Garcia-Sosa[4], Hannes Kollist[1#]

[1]Institute of Technology, University of Tartu, Nooruse 1, Tartu 50411, Estonia.
[2]Institute of Transformative Bio-Molecules, Nagoya University, Furocho, Chikusa, Nagoya, Aichi 464-8601, Japan
[3]School of Biological Sciences, Cell and Developmental Biology Department, University of California San Diego, La Jolla, CA 92093-0116, USA
[4]Institute of Chemistry, University of Tartu, Ravila 14a, Tartu 50411, Estonia
* These authors contributed equally to this study

[#]**Author for correspondence:**

Hannes Kollist,

hannes.kollist@ut.ee

Tel: +372 56470471

Summary

- Protein phosphorylation by kinases is a major molecular switch mechanism involved in the regulation of stomatal opening and closure. Previous research defined interaction between MAP kinase 12 and Raf-like kinase HT1 as a required step for stomatal movements by changes in CO_2 concentration. However, whether MPK12 kinase activity is required for regulation of CO_2-induced stomatal responses warrants in depth investigation.
- We apply genetic, biochemical, and structural modeling approaches to examining the non-catalytic role of MPK12 in guard cell CO_2 signaling that relies on allosteric inhibition of HT1.
- We show that CO_2/HCO_3^--enhanced MPK12 interaction with HT1 is independent of its phosphor-transfer activity. By analyzing gas exchange of plant lines expressing various kinase-dead and constitutively active versions of MPK12 in a plant line where *MPK12* is deleted, we confirmed that CO_2-dependent stomatal responses rely on MPK12's ability to bind to HT1 but not its kinase activity. We also demonstrate that purified MPK12 and HT1 proteins form a heterodimer in the presence of CO_2/HCO_3^- and present structural modeling that explains the MPK12:HT1 interaction interface.
- These data add to the model that MPK12 kinase-activity-independent interaction with HT1 functions as a molecular switch by which stomatal guard cells sense changes in atmospheric CO_2 concentration.

Key words: allosteric inhibition, CO_2 signaling, guard cell, HT1, MAP kinase 12, non-catalytic activity, stomata

Introduction

Carbon dioxide (CO_2) is not only the main substrate for photosynthesis providing food and fiber to virtually all non-autotrophic organisms, but it is also a major signaling molecule used by many domains of life (Foyer & Noctor, 2020; Hall et al., 2010; Phelan et al., 2021). In plants, CO_2 controls opening and closure of stomatal pores, which are formed by a pair of guard cells. These highly specialized guard cells can sense both environmental and endogenous signals, and integrate this information to adjust plant gas exchange with the atmosphere. For optimal growth or even survival, plants have to balance the needs of CO_2 uptake and the risk of losing excess water by transpiration. This is achieved by a guard cell signaling network mainly determined by the crosstalk between CO_2 and other major factors, such as water availability, light and pathogen attack. Therefore, stomatal responses to changes in CO_2 concentration are important as they control both water-use efficiency and carbon cycling in ecosystems.

A key event in guard cell CO_2-sensing involves Mitogen-activated Protein Kinases (MPKs) 12/4 (Marten et al., 2008; Jakobson et al., 2016; Tõldsepp et al., 2018) that can inhibit Raf-like protein kinase High-leaf Temperature 1 (HT1) (Hõrak et al., 2016; Takahashi et al., 2022). HT1 was identified in a screen for mutants that did not respond to changes in CO_2 concentration (Hashimoto et al., 2006). Plants with recessive or dominant mutations in *HT1* lack stomatal movements in response to CO_2 changes, but display normal responses to other environmental factors and abscisic acid (Hashimoto-Sugimoto et al., 2016; Hashimoto et al., 2006; Hõrak et al., 2016). Screening natural variants among *Arabidopsis* accessions uncovered MPK12 as an important component of plant water-use and stomatal responses to CO_2 (Marais et al., 2014; Jakobson et al., 2016). A glycine to arginine substitution (G53R) in the Cvi-0 MPK12 as well as complete deletion of the *MPK12* locus in the Col-0 accession resulted in constitutively more open stomata and reduced stomatal CO_2 responsiveness (Jakobson et al., 2016). Deletion of *MPK12* combined with guard cell-specific suppression of its close homolog, *MPK4*, abolished CO_2-dependent stomatal responses, but retained wild-type (wt)-like responses to other environmental factors and abscisic acid (Hõrak et al., 2016; Tõldsepp et al., 2018). Both MPK12 and MPK4 can interact with HT1 and inhibit HT1 kinase activity *in vitro* (Hõrak et al., 2016; Jakobson et al., 2016). As an active kinase, HT1 was capable of phosphorylating the Slow Anion Channel 1 (SLAC1) (Hõrak et al., 2016), Guard cell Hydrogen peroxide-Resistant 1 (GHR1) (Hõrak et al., 2016; Sierla et al., 2018), and two other Raf-like kinases, the Convergence of Blue light and CO_2 (CBC) 1 and 2 (Hiyama et al., 2017). However, no biological phosphorylated substrate of MPK12 has been found so far, and the purified recombinant MPK12 protein from *E. coli* generally displayed weak autophosphorylation and no detectable transphosphorylation activity (Hõrak et al., 2016; Jakobson et al., 2016; Tõldsepp et al., 2018). MPK12 was shown to phosphorylate artificial substrates only when pulled down from plant cells expressing an epitope-fused MPK12 (Jammes et al., 2009; Lee et al., 2009).

94 Despite their quintessential roles in phosphor-transfer reactions, MPKs and other protein kinases have
95 recently gained attention in their additional, or sometimes even more prominent, non-catalytic roles in
96 signal transduction (Kung & Jura, 2016; Mace & Murphy, 2021; Matallanas et al., 2011). In most cases,
97 these kinases serve as allosteric regulators to other proteins *via* various mechanisms, whereas some
98 protein kinases were found to modulate transcription by interacting with transcription factors
99 independent of their catalytic activities or even direct binding to DNAs (Hu et al., 2009; Madhani et al.,
100 1997).

101 A very recent study identified a mechanism of CO_2 sensing in guard cells in which elevated
102 CO_2/bicarbonate (HCO_3^-) concentration enhanced the interaction of MPK4 and MPK12 with the HT1
103 kinase, thereby down-regulating HT1-dependent phosphorylation and activation of the downstream
104 kinase CBC1 (Takahashi et al., 2022). A model where MPK12/MPK4:HT1 functions as a CO_2/HCO_3^-
105 sensor was proposed and supported by mutations in HT1 (Takahashi et al., 2022). Interestingly, a kinase
106 dead MPK12 was shown to be still functional in mediating CO_2 responses, suggesting a non-catalytic
107 role of MPK12 (Takahashi et al., 2022). However, further research is needed to examine this model of
108 a non-canonical MAP kinase function and to verify MPK12's mode of action in stomatal CO_2 signaling.

109 Here, we apply genetic, biochemical, and structural modeling approaches to investigating the non-
110 catalytic role of MPK12 in the guard cell CO_2 sensing that relies on allosteric inhibition of HT1. We
111 also demonstrate direct CO_2/HCO_3^--dependent dimerization of MPK12 and HT1. Furthermore, we show
112 that MPK4, but not MPK11, can complement loss of MPK12 in the guard cells, further supporting the
113 role of MPK12/4:HT1 interaction as a primary CO_2/HCO_3^- sensor in stomatal guard cells.

114

115 ## Materials and methods

116 ### Molecular cloning

117 For protein expression in *Escherichia coli*, coding sequences of *MPK12* (At2g46070.1) variants with a
118 stop codon were PCR-amplified and cloned at the *Bam*HI/*Eco*RI site of pET28-a vector to create 6xHis-
119 tagged recombinant proteins. Point mutations of *MPK12* were introduced by a two-step overlap-PCR.
120 Constructs of His-tagged HT1 (At1g62400.1) and GST-tagged CBC1 (At3g01490.1) were described in
121 Takahashi et al. (2022). For all other constructs used in this study, simplified diagrams can be found in
122 Figure **S1** with more detailed description in the supplementary methods.

123 ### Protein purification from *E. coli* and *in vitro* kinase assay

124 Recombinant proteins were produced using an *E. coli* protein expression system. Briefly, bacteria were
125 grown in LB or 2xYTQ11 medium at 37°C until the optical density at 600 nm (OD_{600}) reached ~0.5 to
126 0.7, then 0.5 mM isopropyl-β-d-thiogalactopyranoside was added, and *E. coli* were incubated at 20°C

127 for 16 to 24 hours. *E. coli* cells were harvested by centrifugation at 2000g for 20 min and resuspended
128 in Tris-buffered saline [50 mM Tris-HCl (pH 7.5) and 150 mM NaCl]. The *E. coli* cells were disrupted
129 by ultrasonication, and extracted proteins were separated from cell debris by centrifugation at 14,000g
130 for 10 min. GST-tagged proteins and His-tagged proteins were purified using glutathione Sepharose
131 beads and Ni resin beads, respectively.

132 The *in vitro* kinase assays were performed as follows. For the CBC1 phosphorylation assays, 0.5 µg
133 GST-CBC1, 0.01 µg His-HT1 and 0.5 µg His-MPK12 recombinant proteins were incubated in
134 phosphorylation buffer [50 mM Tris-HCl (pH 7.5), 10 mM $MgCl_2$, 0.1% Triton X-100, and 1 mM
135 dithiothreitol (DTT)] with 20 mM $NaHCO_3$ or 20 mM NaCl as a control for 30 min, and then proteins
136 were further incubated with 200 µM ATP and 1 µCi [γ-^{32}P]-ATP for 30 min. For the MPK12 auto-
137 phosphorylation assays, 2 µg His-MPK12 proteins were incubated in MPK phosphorylation buffer [50
138 mM tris-HCl (pH 7.5), 10 mM $MgCl_2$, 10 mM $MnCl_2$, 0.1% Triton X-100, and 1 mM DTT] with 200
139 µM ATP and 5 µCi [γ-^{32}P]-ATP for 60 min.

140 **Tandem affinity purification of HT1 and MPK12 heterocomplex**

141 The baculovirus containing either His-mCherry-HT1 or twin strep-mVenus-MPK12 was constructed
142 using the Bac-to-Bac™ system (Thermo Scientific). Resulting baculoviruses were used to co-infect 600
143 ml of Sf9 insect cells in the shaker culture at the density of $2x10^6$ cells/ml at approximate multiplicity
144 of infection 5-10. Cells were grown for 48 hrs, harvested by centrifugation, washed once with ice cold
145 PBS and resuspended in 30 ml of lysis buffer (50 mM Hepes, pH 7.6; 15 mM NaCl; 10% glycerol;
146 0.5% Tween 20; 10 mM imidazole; 1 mM DTT; 20 mM $NaHCO_3$; Roche protease inhibitors cocktail
147 without EDTA). The resulting cell suspension was flash-frozen in liquid nitrogen and stored at -80°C
148 until needed.

149 To purify the HT1 and MPK12 complex, the cells were thawed and additionally broken in 40 ml Dounce
150 glass homogenizer with 15 strokes of B pestle (all the protein purification steps were carried out either
151 on ice or at 4°C). 5 M NaCl was added to adjust the concentration of this salt to 300 mM and the lysate
152 was cleared by centrifugation at 50000g for 25 min. The cleared lysate was passed through 1 ml of
153 PureCube Ni-NTA agarose column (Cube Biotech). The column was washed three times with N300
154 (50mM Hepes*NaOH pH 7.6; 300 mM NaCl; 10% glycerol; 0.05% Tween 20; 0.2 mM PMSF; 10 mM
155 imidazole; 1 mM DTT; 20 mM $NaHCO_3$) and twice with N100-Ni washing buffer (the same as N300,
156 but with 100 mM NaCl and no PMSF). Proteins were then eluted from the column with N100-Ni buffer
157 + 300 mM imidazole. The eluate was passed through another 0.3 ml Strep-Tactin XT 4Flow column.
158 This was followed by four washes with N100-strep buffer (the same as N100-Ni, but with 25 mM
159 Hepes*NaOH pH 7.6 and no imidazole) and bound protein was eluted from the column with N100-
160 strep + 50 mM biotin buffer. Resulting protein fractions were snap frozen in liquid nitrogen and stored
161 at -80°C.

162 **Size exclusion chromatography**

163 For the -HCO3- analysis, 400 µg of the tandem affinity purified His-mCherry-HT1 + twin-strep-
164 mVenus-MPK12 protein complex in 140 µl volume was mixed with 400 µl of S200 column buffer
165 (25mM Hepes*NaOH pH 7.6; 100 mM NaCl; 1 mM DTT) and concentrated to approximately 50 µl in
166 Amicon Ultra 0.5 ml Ultracel 10k centrifugation tube. This concentrate was mixed again with 500 µl
167 of S200 buffer and concentrated to 30-40 µl before injecting 30 µl of the final preparation into Superdex
168 200 5/150 GL size exclusion column. The column was run with S200 buffer at 50 µl/min and 50 µl
169 fractions were collected. Samples from the peak fractions were analyzed by the 10% polyacrylamide–
170 SDS gel electrophoresis and Coomassie brilliant blue staining of the resolved proteins.

171 For the +HCO3- analysis, the same tandem affinity purified HT1+MPK12 preparation was subjected
172 to the exact same procedure, except that the S200 buffer used in all steps was supplemented with 20
173 mM NaHCO3.

174 **Split-ubiquitin yeast-two hybrid (Y2H) assay**

175 The HT1/pDHB1 bait plasmid was transformed into yeast NMY51 (mating type a) while MPK/pPR3-
176 N prey plasmids were transformed into NMY61 (mating type α). For each pairwise interaction assay,
177 pools of prey transformed NMY61 colonies were mated with a single HT1-transformed NMY51 colony,
178 and the mated diploid cells were selected on SD-LeuTrp plates. Ten to 20 colonies were pooled in
179 overnight liquid cultures (SD-LeuTrp) for growth assays. Three µl of serial dilutions (OD_{600}=0.5, 0.05,
180 and 0.005) were spotted on SD-LeuTrp and SD-LeuTrpHisAde plates and incubated at 37°C for 3 days
181 and then photographed.

182 For quantitative β-galactosidase assays, 100 µl of 3 independent pools of diploid yeast cells (OD_{600}=1)
183 were mixed with 100 µl of Y-PER reagent:2X β-Galactosidase Assay Buffer (1:1) using the Yeast β-
184 Galactosidase Assay Kit (Thermo Scientific) in a 96-well plate, and OD_{414} were measured with a
185 Multiskan FC device (Thermo Scientific) in a 2-5 min interval for 1-2 hrs. A time point where the
186 highest reading was around 1 was selected for calculating β-galactosidase activities for all samples after
187 subtracting blanks where no yeast cells but culture medium was added in the well. Relative β-
188 galactosidase activities were calculated against the positive control of cells containing HT1/pDHB1 and
189 pAI-Alg5 plasmids.

190 **Bimolecular fluorescence complementation (BiFC) assays**

191 For ratiometric BiFC, a total of four *Agrobacterium* GV3101 strains each carrying a *X-YFPn*, *Y-YFPc*,
192 *SLAC1-CFP* or *P19* gene silencing suppressor were co-infiltrated to leaves of 4- to 5-week-old
193 *Nicotiana benthamiana* plants at an OD_{600} of 0.02 for each strain in an infiltration buffer (10 mM $MgCl_2$,
194 10 mM MES, pH 5.6, 200 µM acetosyringone). For CO_2-dependent ratiometric BiFC experiments,
195 infiltrated plants were incubated in an eight-chamber gas-exchange system where each chamber can be

196 set to either high (800 ppm) or low (100 ppm) CO_2 for 3 days. Fluorescence imaging was acquired with
197 a Zeiss LSM710 confocal microscope equipped with a 20x objective at 3-day post infiltration. Before
198 confocal microscopy, leaves subjected to low CO_2 treatment were excised and quickly transferred to a
199 portable box where CO_2 was kept at 100 ppm until imaging. The YFP signals were excited by a 514 nm
200 laser, and emission between 518 and 564 nm was collected. The CFP signals were excited by a 405 nm
201 laser, and emission at 460 to 530 nm was collected. The YFP and CFP signals were collected by
202 sequential scanning to avoid bleed through. Laser power was set to minimize saturation of fluorescence
203 intensity based on the HT1-YFPn and MPK12-YFPc pair, and all parameters were kept identical for
204 the remaining samples.

205 For the CO_2-dependent wide field fluorescence microscopy BiFC experiments at UCSD, a single
206 plasmid containing *35S:HT1-NmVen210*, *35S:MPK12-CVen210* and a *P19* silencing suppressor was
207 transformed to *Agrobacterium tumefaciens* GV3101. *N. benthamiana* plants were grown in standard
208 potting soil (Sungrow Horticulture, Professional Growing Mix, MA, USA) under long-day conditions
209 (16-hr-light/8-hr-dark cycle, 22°C) and 60% relative air humidity. Leaves of 5- to 6-week-old plants
210 were infiltrated with agrobacterial inoculants at an OD_{600} of 0.5, which were blinded by a non-
211 coauthor/non-collaborating laboratory member and only unblinded for a third laboratory member after
212 all analyses of blinded data were completed by the experimenter as in Takahashi et al. (2022). For low
213 CO_2 experiments, plants grown under the above conditions were exposed to low CO_2 for 2 hrs before
214 infiltration and then incubated in a growth chamber (Percival, IntellusUltra AR-41L2) after infiltration,
215 under low CO_2 conditions (100 ppm) for 3 days under constant light conditions at 22°C and 60% relative
216 air humidity. For high CO_2 experiments, the low CO_2-treated plants were subjected to elevated CO_2 in
217 a growth chamber for 2 hrs to 800 ppm CO_2. Microscopy was performed 3 days after infiltration with
218 a Nikon Eclipse E600 fluorescence microscope using a 20x objective lens with an attached INFINITYX
219 digital charge-coupled device color microscopy camera (Takahashi et al., 2022). During microscopy of
220 low CO_2 samples, plants were gassed continuously with low CO_2 by passing filtered air through CO_2
221 absorbent to maintain the CO_2 concentration close to nominally 100 ppm. The mVenus signals were
222 excited by a 515 nm laser, and emission between 528 nm was collected. For each leaf, images from
223 non-overlapping areas were captured. For each image, four points from non-overlapping areas were
224 analyzed. Images were obtained and shown using constant imaging conditions. The fluorescence
225 intensity of the images was measured using ImageJ software.

226 **Western blot analyses**

227 For split-ubiquitin Y2H assays, about 2.5 OD_{600} of yeast cells were harvested by centrifugation and
228 resuspended in 100 µl distilled water and 100 µl of 0.2 M NaOH, incubated for 5 min at room
229 temperature, pelleted, resuspended in 50 µl SDS sample buffer (0.06 M Tris-HCl, pH 6.8, 5% glycerol,
230 2% SDS, 4% β-mercaptoethanol, 0.0025% bromophenol blue) and boiled for 10 min (Kushnirov, 2000).

231 For ratiometric BiFC experiments, leaf samples (50 mg) were ground under liquid nitrogen and boiled
232 in 100 µl extraction buffer (0.1 M EDTA, pH 8.0, 0.12 M Tris-HCl, pH 6.8, 4% w/v SDS, 10% v/v β-
233 mercaptomethanol, 5% v/v glycerol, 0.005% w/v bromophenol blue) for 10 min (Tsugama et al., 2011).
234 Thirty µl of each sample were separated on a 10% SDS polyacrylamide gel. After electrophoresis, total
235 proteins were transferred onto a nitrocellulose membrane and stained with Ponceau S. Immunodetection
236 of HA-tagged proteins was carried out with a monoclonal anti-HA antibody followed by a goat
237 horseradish peroxidase-conjugated secondary antibody and chemiluminescent detection.

238 **Plant maintenance and gas-exchange experiments**

239 The *Arabidopsis thaliana MPK12*-deletion (*mpk12-4*) is in the Col-0 accession background, and was
240 isolated previously (Jakobson et al., 2016). Transgenic plants with various binary constructs were
241 generated in the *mpk12-4* background.

242 For the CO_2 response phenotyping, seeds were stratified for 2-4 days at 4°C and sown in
243 peat:vermiculite (2:1) mixture in a glass-covered pot to allow separation of rosette leaves from the root
244 and growth media during gas-exchange experiments (Kollist et al., 2007). The plants were cultivated in
245 growth chambers with the following growth conditions: 10/14 hrs light/darkness with 23/19°C and
246 ~60%/80% relative air humidity for light/darkness periods, respectively, and a photosynthetic photon
247 flux density of 250 µmol photons m^{-2} s^{-1}. Three- to four-week-old plants were analyzed in an eight-
248 chamber gas-exchange measurement system Jyrkki (PlantInvent Ltd.) under conditions similar to the
249 growing period. Plants were allowed to be acclimated in the system under 420 ppm CO_2 for about 2 hrs
250 until a steady-state stomatal conductance was reached before applying CO_2 changes. Stomatal
251 conductance was then analyzed in a high (800 ppm)/ambient (420 ppm)/low (100 ppm) CO_2 regime
252 with duration of 56 min for each treatment.

253 **Transgenic plant generation and verification**

254 The *Arabidopsis mpk12-4* plants were transformed by the floral dip method (Clough & Bent, 1998).
255 Transgenic seeds were first selected based on the pFAST-R marker (Shimada et al., 2010) that produced
256 red fluorescence in dry seeds. Transgene expression was further verified in the experimental plants'
257 leaves with a Zeiss LSM710 confocal microscope using a 20x objective. The mVenus signals were
258 excited by a 514 nm laser and the emission was collected in the 518-564 nm wave-length range.

259 **Statistical Analyses**

260 Statistical analyses were performed using Statistica, version 7.1 (StatSoft) or GraphPad Prism software
261 (version 8.0.1). One-way or two-way ANOVA analyses with Tukey post hoc tests were used, as
262 indicated in figure legends. All effects were considered significant at $P < 0.05$ unless otherwise stated.

263 **Structural modeling**

264 Sequences for proteins were obtained from the TAIR website (www.arabidopsis.org). AlphaFold2 deep
265 learning prediction of protein structure was performed with ColabFold using MMseq2, both for
266 monomers and multimers, wild-type and mutants (Mirdita et al., 2021, 2022), without the use of
267 AlphaFold Multimer or templates. Amber-Relax was disabled. A separate multiple sequence alignment
268 (MSA) is generated for each protein. The per-residue confidence metrics (pLDDT) and predicted
269 aligned errors (PAE) parameters of quality of fit were followed and assessed. Models were generated
270 and ranked by per-residue confidence metric. Turbo was used, and a maximum number of sequences
271 was set to 512:1024. Deepmind's fine-tuned model parameters were used to obtain the PAE per
272 structure, with one trunk of the network run multiple times with different random choices for the MSA
273 cluster centers, three recycles - times the structure is fed back into the neural network for refinement,
274 in addition to one random number seed. Models were superposed for interface comparison.

275

276 ## Results

277 **MPK12:HT1 interaction does not require MPK12 kinase activity, but depends on specific amino**
278 **acids**

279 We previously demonstrated that interaction between MPK12 and HT1 is strongly impaired with a
280 G53R substitution in MPK12, which was identified in the Cvi-0 natural accession of *Arabidopsis*
281 *thaliana* (Jakobson et al., 2016). *In vitro* kinase assays revealed autophosphorylation activity of
282 MPK12, but not the G53R mutant, implying that loss of kinase activity could affect the interaction.
283 However, a kinase-dead version of MPK12 with arginine substitution to the invariant lysine (K70)
284 required for ATP binding was only slightly impaired in its ability to inhibit HT1 compared to the
285 wtMPK12 and a hyperactive MPK12(Y122C) (Jakobson et al., 2016). These results raised the question
286 of whether MPK12 kinase activity is required for its interaction with HT1. To address this question, we
287 generated another MPK12 mutant with D196G and E200A substitutions, named MPK12(DE). Similar
288 to MPK12(Y122C), MPK12(DE) was designed based on conserved substitutions leading to constitutive
289 active kinases in *Arabidopsis* MPK3/4/6 (Berriri et al., 2012). However, purified recombinant
290 MPK12(DE) showed only weak but comparable autophosphorylation activity to wtMPK12, whereas
291 MPK12(Y122C) yielded a strong autophosphorylation signal in the *in vitro* kinase assay activity (Figure
292 **1a**). On the other hand, the G53R and K70R mutants did not show any detectable autophosphorylation
293 activity (Figure **1a**), consistent with our previous report (Jakobson et al., 2016).

294 We next performed interaction assays between HT1 and all five MPK12 variants. We chose the split-
295 ubiquitin yeast-two-hybrid (Y2H) system due to the membrane association nature of HT1 (Hashimoto-
296 Sugimoto et al., 2016; Hõrak et al., 2016). Consistent with our previous report (Jakobson et al., 2016),
297 wtMPK12, but not its close homolog, MPK11, interacted well with HT1. The G53R kinase-deficient

298 MPK12 and the weakly active MPK12(DE) did not interact with HT1, whereas another kinase-dead
299 version, K70R, and the hyperactive Y122C displayed comparable interactions with HT1 as the
300 wtMPK12 (Figures **1b** & **S1a**). To rule out the possibility that lack of interaction was due to poor or no
301 expression of MPK12 proteins in yeast, we performed western analysis and showed that all baits
302 including five MPK12 variants and MPK11 were well expressed (Figure **S2a**).

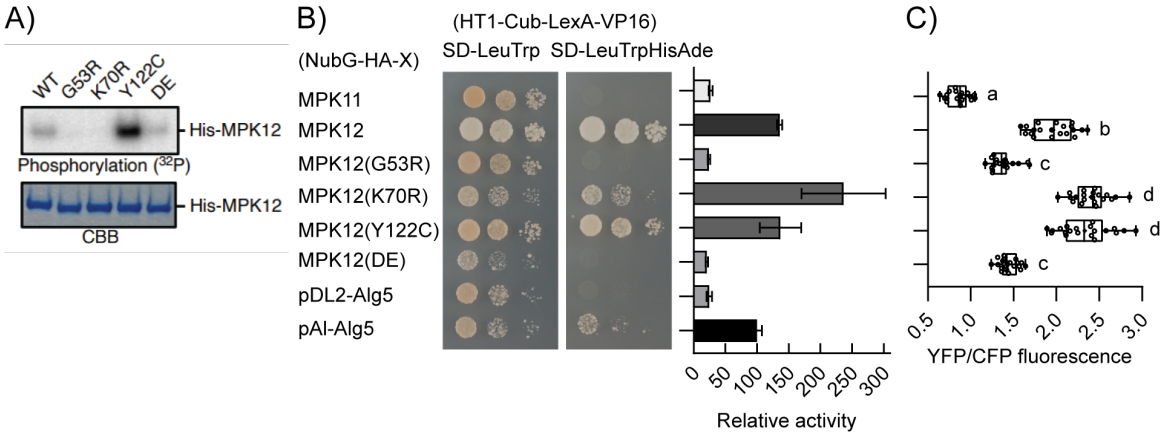

Figure 1. MPK12 interaction with HT1 does not depend on MPK12 kinase activity.

A) Kinase activity of MPK12 and its variants: WT and DE versions of MPK12 displayed weak autophosphorylation, whereas the Y122C variant had a higher activity; no autophosphorylation activity of the G53R and K70R versions was detected; MPK12 autophosphorylation levels (upper panel) and Coomassie brilliant blue (CBB)-stained gels (lower panel) are shown; the illustrated experiment was repeated 3 times with similar results.
B) Split-ubiquitin yeast two-hybrid (Y2H) assay: yeast growth with serial dilution on a SD-LeuTrp plate indicates presence of both bait (HT1-Cub-LexA-VP16) and prey (NubG-HA-X) plasmids, and on a SD-LeuTrpHisAde plate to select for interaction; only MPK12, MPK12(K70R) and MPK12(Y122C) interact with HT1; pDL2-Alg5 and pAI-Alg5 are negative and positive prey controls, respectively; bar graph shows relative β-galactosidase activities normalized by the positive control; error bars are SEM (n=3).
C) Ratiometric bimolecular fluorescence complementation (BiFC) assay in *Nicotiana benthamiana*: box & whisker plot shows stronger interaction between HT1 and MPK12, MPK12(K70R) and MPK12(Y122C); y-axis depicts the split-YFP pairs (HT1-YFPn + MPK-YFPc) used for leaf infiltration, along with *Agrobacterium* carrying a *SLAC1-CFP* construct as a control; x-axis is the ratio of YFP and CFP fluorescence, which indicates interaction strength normalized by the SLAC1-CFP reference control; 20 confocal images taken from three independent leaves were analyzed for each interaction pair; statistically significant groups are denoted with different letters (One-Way ANOVA with Tukey HSD *post hoc* test, $P < 0.05$).

303 We also checked the interaction of HT1 and the MPK12 variants in *Nicotiana benthamiana* by the
304 ratiometric bimolecular fluorescence complementation (BiFC) assays. A SLAC1-CFP fusion, which is
305 localized to the plasma membrane where the HT1:MPK12 interaction mainly takes place, was used as
306 a reference control to normalize the BiFC signals (Figure **S1b**). In agreement with the Y2H results, in
307 addition to wtMPK12, the K70R and Y122C variants showed strong interaction with HT1 as indicated
308 by the higher ratio of YFP/CFP fluorescence. On the other hand, the G53R and DE versions of MPK12,
309 as well as MPK11, had very low YFP/CFP signals (Figures **1c** & **S1b**). All split YFP fusion proteins
310 were well expressed as verified by western blot analysis (Figure **S2b**). These data using independent

311 approaches support the model that HT1:MPK12 interaction is independent of MPK12 kinase activity,
312 and the interaction interface may include the G53, D196, and E200 amino acids.

313 **Kinase activity-independent interaction between MPK12:HT1 depends on CO_2/HCO_3^-**
314 **concentration**

315 Both Y2H and BiFC assays allow interaction studies with only a static view due to their irreversibility.
316 Despite the limitation, the irreversible nature of these assays could enhance transient interactions. We
317 modified the BiFC experiments by growing *N. benthamiana* plants under either elevated (800 ppm) or
318 reduced (100 ppm) CO_2 conditions post-infiltration to capture potential CO_2-dependent MPK12:HT1
319 interaction. Using our modified ratiometric BiFC assays, an increase of YFP/CFP signal was observed
320 for wtMPK12 and HT1 under 800 ppm CO_2 compared to that under 100 ppm. This high CO_2-induced
321 signal increase was absent for MPK12(G53R), which had weak interaction signals under both high and
322 low CO_2 conditions (Figure **2a**). Similarly, widefield microscopy-based BiFC assays were conducted
323 with inoculation and subsequent growth at low, 100 ppm, CO_2, followed by continuous gassing with
324 low CO_2 air during fluorescence imaging for the low CO_2-treated samples. These experiments also
325 revealed high CO_2-induced MPK12:HT1 interaction, which was abolished by the G53R mutation in
326 MPK12 (Figures **2b** & **S1c**). We previously reported that HT1 inhibited SLAC1, whose activation led
327 to stomatal closure, and this inhibition by HT1 was suppressed by MPK12:HT1 interaction (Hõrak et
328 al., 2016). Very recently, we uncovered CO_2/bicarbonate (HCO_3^-)-induced inhibition of CBC1
329 phosphorylation by HT1 when MPK12 was added to the reaction, and proposed that MPK12 and
330 MPK4, together with HT1 form the primary CO_2/HCO_3^- sensor in the guard cells (Takahashi et al.,
331 2022). In order to further investigate whether MPK12-induced inhibition of CBC1 phosphorylation by
332 HT1 requires MPK12 kinase activity or only its binding to HT1, we performed *in vitro* kinase assays
333 with the five versions of MPK12 at elevated or low CO_2/HCO_3^-. This experiment showed that 20 mM
334 of CO_2/HCO_3^- inhibited CBC1 phosphorylation in the presence of HT1 plus wtMPK12, consistent with
335 the recent study (Takahashi et al., 2022). Interestingly, the MPK12(K70R) and MPK12(Y122C) mutant
336 proteins also inhibited CBC1 kinase activity, but not the G53R and DE variants (Figure **2c**). These
337 results support a critical role of MPK12:HT1 interaction in the CO_2/HCO_3^--sensing mechanism and its
338 independence of MPK12 kinase activity.

339 **Purified MPK12 and HT1 form a heterodimer in the presence of bicarbonate**

340 To carry out more direct binding assays for MPK12 interaction with HT1 and its dependence on
341 CO_2/HCO_3^- concentration, we sought additional systems for protein purification due to difficulties of
342 expressing HT1 in *E. coli*. We co-expressed HT1 and MPK12 proteins in insect cells using the
343 baculovirus expression system followed by tandem purification (Figure **S1d**). During the entire
344 purification process, 20mM of $NaHCO_3$ was added to enhance the MPK12:HT1 complex formation.

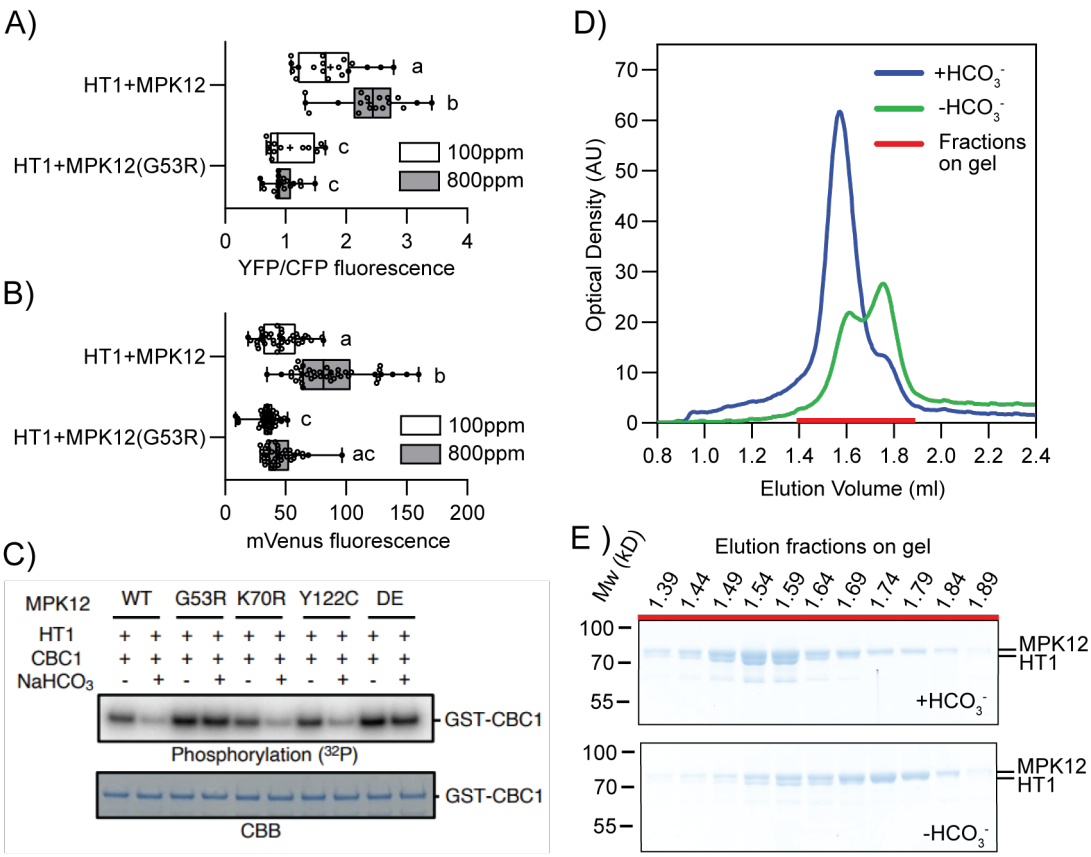

Figure 2. MPK12 interacts with HT1 and inhibits CBC1 phosphorylation by HT1, which are dependent on CO_2/HCO_3^- concentrations and specific amino acids in MPK12

A) Ratiometric confocal microscopy-based BiFC assays in *N. benthamiana* plants kept under reduced (100 ppm) and elevated (800 ppm) CO_2 conditions after infiltration: MPK12, but not MPK12(G53R), displays increased interaction to HT1 under 800 ppm CO_2; y-axis indicates split YFP pairs, and x-axis is YFP signal normalized to the SLAC1-CFP reference control; statistically significant groups are denoted with different letters (two-way ANOVA followed by Tukey's multiple comparisons test; $P < 0.005$, n=12 for MPK12(G53R) at 100 ppm CO_2, and 18 for all others).
B) Widefield microscopy-based BiFC in *N. benthamiana* infiltrated and subsequently grown at 100 ppm CO_2 for 3 days, and then exposed to 800 ppm or continuing at 100 ppm: MPK12 displays high CO_2-induced interaction to HT1, which is not evident in the G53R mutant; y-axis shows split mVenus pairs, and x-axis is the mVenus fluorescence intensity; statistically significant groups are denoted with different letters (two-way ANOVA followed by Tukey's multiple comparisons test; $P < 0.05$; n=40).
C) CBC1 phosphorylation by HT1 is reduced by WT, K70R and Y122C versions of MPK12, but not the G53R and DE variants under elevated CO_2/HCO_3^- condition; His-MPK12s, His-HT1 and GST-CBC1 recombinant proteins were incubated with or without 20 mM $NaHCO_3$ for 30 min, and then *in vitro* phosphorylation analyses were performed by adding ^{32}P-ATP; CBC1 phosphorylation levels and Coomassie brilliant blue (CBB)-stained gels are shown.
D) Elution profiles of the Superdex 200 5/150 GL size exclusion chromatography of the His-mCherry-HT1 + twin strep-mVenus-MPK12 protein complex; the same tandem affinity purified protein preparation, purified in the presence of 20mM NaHCO3, was used in both $+HCO_3^-$ and $-HCO_3^-$ runs.
E) Coomassie brilliant blue stained 10% polyacrylamide-SDS gels showing total proteins in the peak fractions of the chromatography runs depicted in **d)**; the starting elution volumes of the sampled chromatography fractions are indicated on top of each lane; the molecular weight (Mw) standards are indicated on the left; expected Mw of the His-mCherry-HT1 and twin strep-mVenus-MPK12 proteins are 72.9kD and 74.6kD, respectively.

346 The purified complex was then subjected to size exclusion chromatography in the presence or absence
347 of added $NaHCO_3$. As shown in Figure 2d, in the presence of $NaHCO_3$, the main peak is close to the
348 elution volume (Ve) of the 158 kD standard, suggesting that it corresponds to the MPK12:HT1
349 heterodimer (147.5 KD). This peak is significantly diminished and a second peak with Ve towards the
350 smaller size (75 kD) becomes dominant in conditions without $NaHCO_3$, and thus likely corresponds to
351 the mixture of both monomers. The presence of both MPK12 and HT1 in the larger size fraction was
352 confirmed by SDS-PAGE (Figures **2e** & **S3**). These data provide more direct evidence on the
353 CO_2/HCO_3^--dependent interaction between MPK12 and HT1, and suggest a 1:1 stoichiometry in the
354 MPK12:HT1 complex.

355 **MPK12 kinase activity is not required for its function in CO_2-dependent stomatal regulation**

356 Due to the fact that we were unable to detect HT1 phosphorylation by MPK12, it is tempting to speculate
357 that MPK12 exerts its function by sequestering HT1 from phosphorylating downstream effectors
358 independent of the MPK12 phospho-transfer activity. The *mpk12-4* plant, which has the *MPK12* locus
359 completely deleted, together with our five MPK12 variants used in the interaction and kinase assays,
360 provide an excellent platform and tools to address this question. We reasoned that by transforming the
361 *mpk12-4* plants with these MPK12 variants, we could gain insights in the mode of MPK12 function in
362 CO_2 signaling. We designed and prepared three sets of binary constructs as depicted in Figure S4a. Each
363 set included five constructs of different *MPK12* variants, together with a seed-specific red fluorescent
364 protein marker. The first set contained a 2.5 kb of the *MPK12* genomic sequence without any tag
365 (*gMPK12*) to avoid potential disturbance to the native gene function. The second set had a *mVenus* and
366 a *HA* tag fused to the genomic sequence of *MPK12* (*gMPK12-mVenus-HA*) for easier verification of
367 the guard cell-specific MPK12 expression. The last set aimed to express MPK12-mVenus-HA fusion
368 protein in most cell types by placing the coding sequence between an *Arabidopsis ubiquitin 10* promoter
369 (*pUBQ10*) and a *NOS* terminator (*tNOS*) from the *Agrobacterium tumefaciens* (*pUBQ10:cMPK12-*
370 *mVenus-HA_tNOS*). All three sets of constructs were used to generate transgenic plants in the *mpk12-4*
371 background. Several T1 seeds with clear red fluorescence were selected from each of the 15 plant lines,
372 and their stomatal responses to CO_2 changes were examined by a whole plant gas-exchange device
373 (Figure **S4b-d**).

374 Consistent with previous reports (Jakobson et al., 2016; Tõldsepp et al., 2018), the *mpk12-4* plant had
375 strongly reduced responses to both high and low CO_2 levels, and its stomatal conductance was about
376 1.5-fold higher than Col-0 at the ambient CO_2 (420 ppm) condition (Figure **S4b**). The majority of T1
377 plants transformed with the wtMPK12 in all 3 sets of constructs displayed Col-0-like stomatal
378 conductance (Figure **S4b**) and responses to both high and low CO_2 treatments (Figure **S4c,d**), indicating
379 no clear interference to the MPK12 function with the mVenus-HA tag. Among the four MPK12

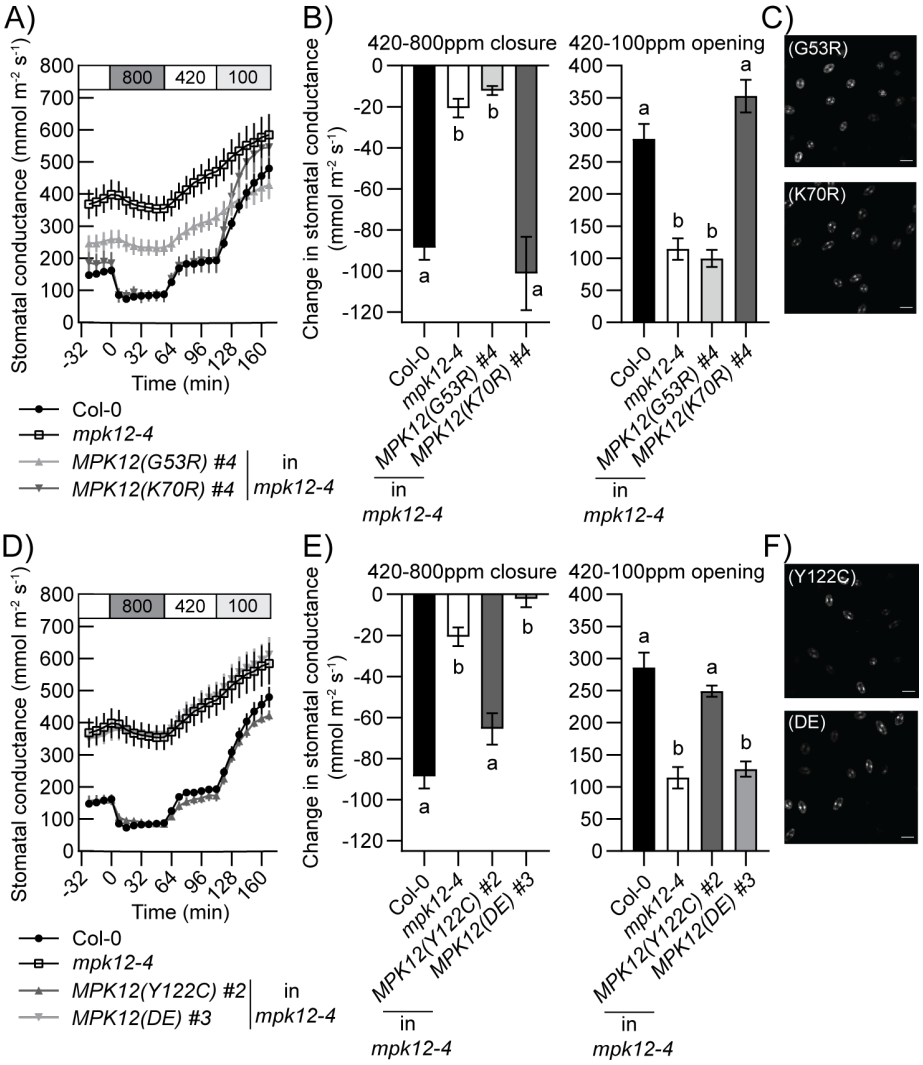

Figure 3. Kinase activity of MPK12 is not required for CO_2 induced stomatal movements.

A, D) Time-resolved patterns of whole-plant stomatal conductance in response to changes in CO_2 concentrations (in parts per million; ppm) as indicated on top of the panels; intact plants of Col-0 (n=13), *MPK12* deletion line *mpk12-4* (n=12), and *mpk12-4* transformed with *MPK12(G53R)* (n=7), *MPK12(K70R)* (n=5) in **a)** and *MPK12(Y122C)* (n=4), *MPK12(DE)* (n=5) in **d)** were analyzed; data of Col-0 and *mpk12-4* controls are the same in **a** & **d** as they were obtained in the same experimental set.
B, E) Stomatal closure at 16 min after application of 800 ppm CO_2 (left panels) and stomatal opening after application of 100 ppm CO_2 for 56 min (right panels); statistically significant groups are denoted with different letters (ANOVA with Tukey HSD unequal N post hoc test, $P < 0.05$).
C, F) Representative confocal micrographs of guard cell-specific expression of MPK12 variants fused to mVenus in each transgenic line; scale bar=20 µm.

380 mutants, only those capable of interacting with HT1 (K70R and Y122C), regardless of their kinase
381 activities, could restore CO_2 responses in the *mpk12-4* background (Figure **S4c,d**).

382 We then focused on the set of *gMPK12-mVenus-HA* plants and selected two independent T2 lines from
383 each MPK12 variant for further study. Consistent with the results in T1 plants, only plants with the
384 wtMPK12, K70R and Y122C mutants complemented the *mpk12-4* phenotype with respect to their
385 stomatal CO_2 responses and the steady state conductance at ambient CO_2 (Figures **3** & **S5**).

386 Interestingly, despite having impaired CO_2 responses similar to the *mpk12-4* plants, T2 plants with the
387 G53R and DE versions of MPK12 had lower stomatal conductance than the *mpk12-4* plants (Figures
388 **3a,d** & **S5a,c**). Expression of the MPK12 variants was verified by confocal microscopy based on the
389 mVenus fluorescence, and was found to be guard cell-specific as expected for the native *MPK12*
390 promoter (Figure **3c,f**). All these results clearly suggest a catalytic-independent role of the MPK12 in
391 guard cell CO_2 signaling.

392 **A MPK12:HT1 structural modeling reveals important MPK12 amino acids at the interaction**
393 **interface with HT1**

394 We constructed a predicted complex system of MPK12:HT1 using AlphaFold2 (Jumper et al., 2021).
395 The predicted structure for the MPK12:HT1 complex showed good per-residue confidence metrics,
396 with the residues in the interface area all assessed to have high accuracy (deep blue, Figure **4a**). The
397 predicted aligned errors showed low values for residue pairs of interest, predicting well-defined relative
398 positions. The complex is well-folded, with no overly exposed regions. Important tertiary and secondary
399 structures of MPK12 are recognizable, such as smaller N-lobe and larger C-lobe (Figure **4b**). Residues
400 of MPK12 that are modeled to be important for binding along the interface are G53, D196 (hydrogen
401 bond donated from the side-chain oxygen of D196 to the side-chain nitrogen of K91 in HT1), and E200
402 (hydrogen bond from the backbone oxygen of E200 to the side-chain NH_2 of R102 in HT1), along with
403 residues in the substrate binding region: N263, Y277, and P285. Deletion of D196, E200, and G53
404 resulted in a predicted unfavorable binding due to loss of intermolecular contacts, as well as to MPK12
405 function. On the other hand, residues K70 and Y122 are predicted not to be in the contact surface

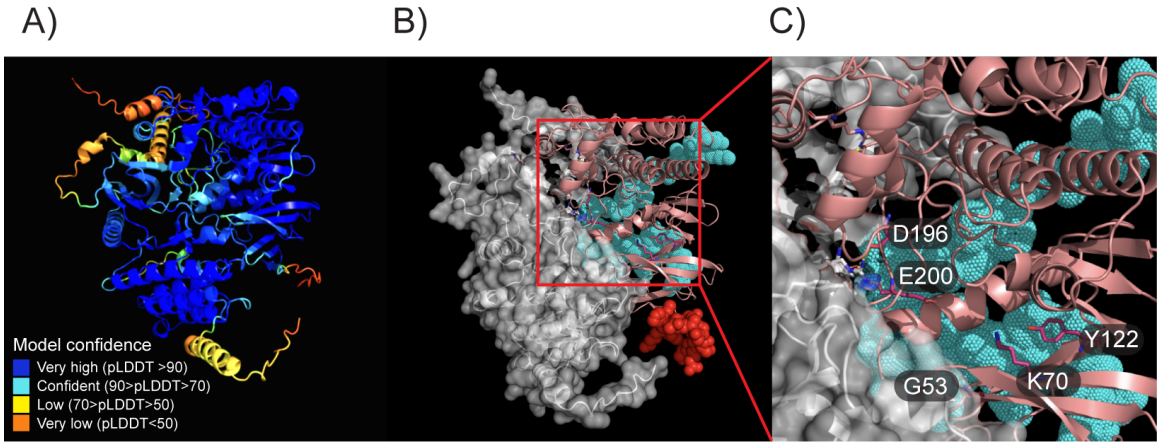

Figure 4. AlphaFold2 structural prediction model for the complex of MPK12 with HT1

A) Color-coded model confidence indicates a very good overall confidence, with very high accuracy at the interface area indicated by the per-residue confidence metrics (pLDDT).
B) HT1 (gray, surface-filled structure) in complex with MPK12 (pink, ribbon structure) with highlights in the N-terminal region (15 amino acids, red spheres), C-terminal region (41 amino acids, cyan dots), and residues G53, K70, Y122, D196, and E200 of MPK12.
C) Closeup of the interaction interface highlighting MPK12 interface residues G53, D196, and E200, and MPK12 non-interface residues K70 and Y122, of MPK12.

between MPK12 and HT1 (Figure **4c**), and their mutation also does not affect physiological functions (Figures **3**, **S4** & **S5**).

MPK4, but not MPK11, complements *MPK12*-deletion phenotype

There are 20 *MPK*s in the *Arabidopsis* genome, which can be further separated into four (A to D) subgroups based on sequence homology. *MPK12* is most highly similar to *MPK4* and *MPK11* in the subgroup B (Hamel et al., 2006; Ichimura et al., 2002). We have previously shown that *MPK12* is diverged from *MPK4*, and is specific to the Brassicaceae among angiosperms (Tõldsepp et al., 2018). *MPK12* is principally expressed in the guard cells, whereas *MPK4* is more ubiquitous and has broader functions. Accordingly, deletion of the *MPK12* gene does not affect plant growth, whereas the *MPK4*

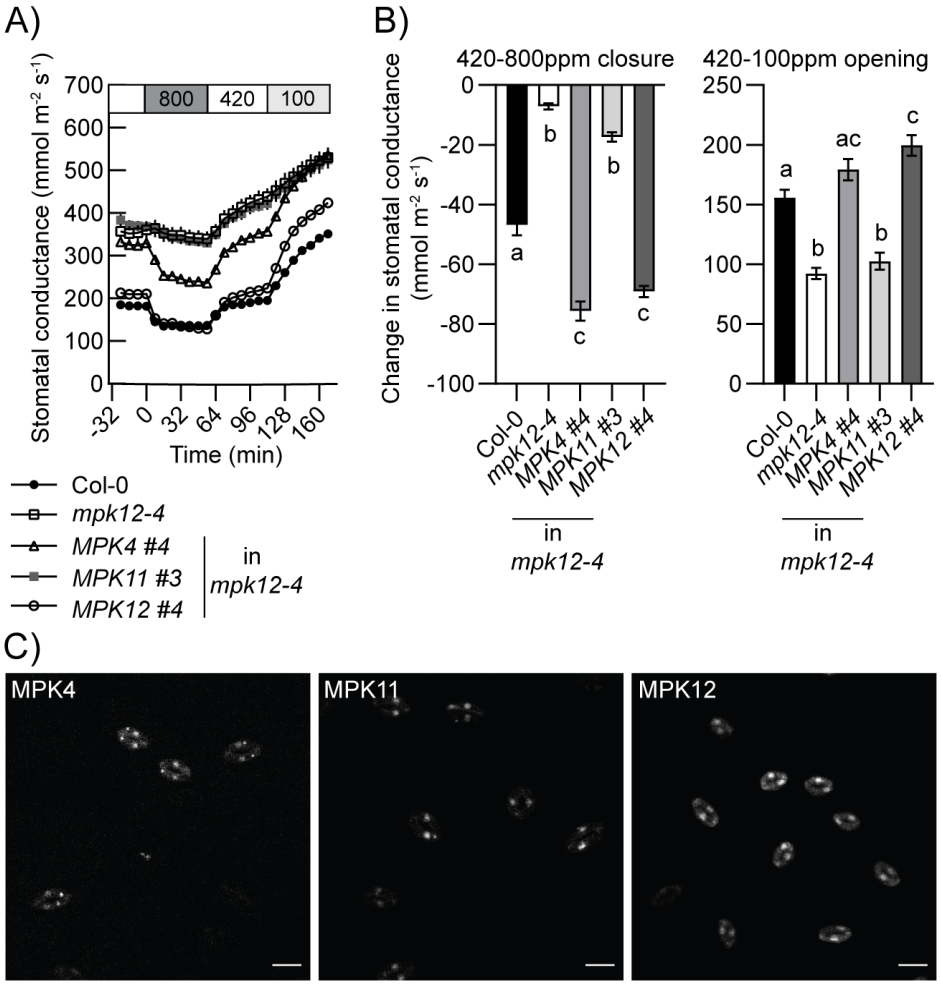

Figure 5. Expression of MPK4 in guard cells can restore *mpk12-4* CO_2 responses.

A) Time-resolved patterns of stomatal conductance in response to changes in CO_2 concentrations (in parts per million; ppm) as indicated on top of the panels of *mpk12-4* plants complemented with *pMPK12:MPK4/11/12-mVenus-HA* constructs and Col-0 plants (n=4-5).
B) Stomatal closure at 16 min after application of 800 ppm CO_2 (left panels) and stomatal opening after application of 100 ppm CO_2 for 56 min (right panels); statistically significant groups are denoted with different letters (ANOVA with Tukey HSD unequal N post hoc test, $P < 0.05$).
C) Representative confocal micrographs of guard cell-specific expression of MPK-mVenus fusion; scale bar=20 µm.

knockout mutants are extremely dwarfed (Petersen et al., 2000; Tõldsepp et al., 2018). Expressing *MPK12* under the *MPK4* promoter could not rescue the dwarfism phenotype, indicating MPK12 has evolved as a more specialized stomatal regulator at the protein level (Tõldsepp et al., 2018). However, it has not been tested whether the more ancient MPK4 or other close homologs, such as MPK11, can substitute the MPK12 function in the guard cells. We fused the coding sequence of *MPK4* or *MPK11* to *mVenus-HA*, and placed it under the control of *MPK12* promoter and terminator. All plants transformed with the *MPK4* construct which displayed guard cell-specific mVenus fluorescence restored the CO_2 responses in the *mpk12-4* background. On the contrary, none of the *MPK11* transgenic plants, despite having clear guard cell mVenus fluorescence, could complement the *mpk12-4* phenotype (Figures **5** & **S6**).

Discussion

In the present study, we characterize a function of MPK12 in stomatal CO_2 sensing that is independent of its kinase activity, but requires interaction with the HT1 in a CO_2/HCO_3^--dependent manner. Our results with point mutations in MPK12 (Figures **1-3** & **S5**), along with recent findings by Takahashi et al. (2022), strongly suggest MPK12 as an allosteric inhibitor for the HT1 kinase. Together these two proteins form a dynamic complex that responds to the intercellular CO_2/HCO_3^- concentration (Figure **2**; Takahashi et al., 2022) and thus modulate stomatal CO_2 responses.

In support of our model that MPK12:HT1 regulates stomatal movements *via* complex formation or dissociation depending on the CO_2 levels, we demonstrate that the phospho-transferase activity of MPK12 can be uncoupled from its ability to interact with HT1 (Figure **1**). The MPK12(G53R) variant was identified from the natural Cvi-0 accession of *Arabidopsis thaliana*, and found to be defective in its kinase activity as well as ability to interact with HT1. The G53 residue is located in the glycine-rich loop (GxGxx**G**) between β1 and β2 in the N-lobe of the bi-lobed protein kinase architecture (Figure **4c**). This loop is the most flexible part in the N-lobe, and is responsible for positioning the γ-phosphate of ATP for catalysis. Another variant, MPK12(K70R), was created by mutating the conserved lysine in the Ax**K** motif in β3, which is also part of the ATP-binding pocket. Substitutions in these regions are frequently found in pseudokinases, and mutations in active kinases normally resulted in kinase deficiency (Taylor & Kornev, 2011). We confirm loss of autophosphorylation in the G53R and K70R versions of MPK12 (Figure **1a**; Jakobson et al., 2016). On the other hand, we generated two versions of "hyperactive" MPK12 based on mutations in corresponding residues that resulted in elevated basal kinase activities of the *Arabidopsis* MPK3/4/6 in yeasts (Berriri et al., 2012). The MPK12(Y122C) has a tyrosine to cysteine conversion at the gatekeeper residue that connects two hydrophobic spines, the regulatory (R) and catalytic (C) spines, and thus regulates ATP binding. Replacing this residue with a bulkier amino acid tends to stabilize the R-spine and favors kinase activation (Taylor & Kornev, 2011).

450 However, in one of the mammalian MPKs, the ERK2, mutations of the gatekeeper glutamine (Q103)
451 to a smaller glycine or alanine increased basal activity due to autoactivation, which was attributed to
452 higher backbone flexibility in the activation lip (Emirick et al., 2006). The conversion from a bulkier
453 tyrosine to smaller cysteine in the Y122C mutant of MPK12 may also lead to autoactivation via a similar
454 mechanism. The DE mutants contained substitutions in two amino acids, and this version of *Arabidopsis*
455 MPK4 exhibited MAP2K-independent activity *in planta*, whereas MPK4(Y124C) was hyperactive
456 when purified from *E. coli*, but not *in planta* (Berriri et al., 2012). Our kinase assay results revealed
457 strong autophosphorylation in the recombinant MPK12(Y122C) purified from *E. coli*, but only weak
458 phosphorylation in MPK12(DE) (Figure **1a**). However, whether MPK12(DE) is hyperactive *in planta*
459 requires further study by purifying proteins from the transgenic plants.

460 In total, we generated five amino acid mutations which are distributed across various conserved
461 domains of the MPK12 and have differential effects on the kinase activity. Our interaction study and *in*
462 *vitro* kinase assays clearly demonstrate that interaction between MPK12 and HT1 can be induced or
463 enhanced by elevated CO_2 or HCO_3^-, and does not require kinase activity of MPK12 (Figures **1** & **2**).
464 Indeed, a computer-based structural modeling maps G53, D196 and E200 in MPK12 to the interface of
465 the MPK12:HT1 complex, whereas MPK12 residues of K70 and Y122 are predicted to be away from
466 the interface (Figure **4**). Structural modeling has also suggested that strong dominant mutations in the
467 HT1 protein lie at the predicted interface of MPK4/MPK12 with HT1 (Takahashi et al., 2022). Together
468 these models, supported by CO_2-induced stomatal movement phenotypes of respective mutant plants,
469 implicate the relevance of the MPK12 and HT1 interface for functional CO_2 signaling. High CO_2
470 concentration may potentially produce changes in binding due to pH modification. These could be
471 changes in ionization states of polar amino acids, as well as chemical modification of specific side
472 chains that could produce inter-residue links.

473 We reasoned that these MPK12 variants, each displaying contrasting features with respect to kinase
474 activity and ability to interact with HT1, could be useful tools in addressing the question: Is MPK12-
475 mediated stomatal CO_2 signaling dependent on the MPK12 catalytic activity or its ability to modulate
476 HT1 *via* allosteric inhibition, or even both? Using the *MPK12*-deletion (*mpk12-4*) line as a platform,
477 we demonstrate full restoration of CO_2 responses in the *mpk12-4* plants complemented with the
478 wtMPK12, MPK12(Y122C), and more importantly, the kinase-dead MPK12(K70R). On the other
479 hand, MPK12(G53R) and MPK12(DE) could not rescue *mpk12-4* CO_2-insensitive phenotype (Figures
480 **3**, **S4** & **S5**). These results are in accordance with the interaction study (Figure **1**) and kinase assays
481 (Figure **2c**), supporting a non-catalytic role of MPK12 in guard cell CO_2 signaling.

482 Eukaryotic protein kinases are enzymes with a highly conserved bilobed protein fold capable of
483 phosphor-transfer *in trans* or *in cis* (*i.e.* transphosphorylation or autophosphorylation). However, unlike
484 other catalytic enzymes, they are very inefficient in terms of catalysis. All protein kinases transition

485 between inactive and active states, yet eukaryotic protein kinases seem to shift the equilibrium mostly
486 towards the inactive state, and only become active transiently under specific conditions (Taylor &
487 Kornev, 2011). Eukaryotic protein kinases often function as molecular switches, resembling the GTP-
488 binding proteins, which regulate a diverse array of biological processes by switching between "on" and
489 "off" states upon GTP binding (Shaw et al., 2014). By acting sequentially, such as in the case of the
490 MAPK cascades which comprise of at least three tiers of kinases, even a weak initial signal can be
491 amplified and transduced to the targeted site. However, compelling evidence has emerged that kinases
492 can carry out important functions beyond phosphorylation. A growing number of mammalian and yeast
493 kinases have been demonstrated to play non-catalytic roles such as being allosteric regulators or
494 scaffolds for specific protein assemblies. The MAP kinase ERK2 was shown to regulate transcription
495 by directly binding to DNA through a cluster of positively-charged amino acids in the C lobe of the
496 kinase domain (Hu et al., 2009). However, no such non-catalytic functions of active plant kinases,
497 except for some instances in pseudokinases (Sierla et al., 2018), has been reported *in vivo*. Our findings,
498 together with Takahashi et al. (2022), represent a founder example of a plant MAP kinase that plays an
499 important function independent of its catalytic activity.

500 We further show that two close homologs of MPK12 display distinct abilities to interact with HT1, and
501 this ability is in accordance to whether they are capable of complementing loss of *MPK12 in planta*.
502 Among the five *Arabidopsis* group B MPKs, MPK4, 11 and 12 share highest homology, yet only MPK4
503 and 12 are able to inhibit HT1 *via* protein-protein interaction (Hõrak et al., 2016; Jakobson et al., 2016;
504 Takahashi et al., 2022). Accordingly, *MPK4*, but not *MPK11*, when driven under the *MPK12* promoter,
505 can restore CO_2 responses in the *mpk12-4* plant (Figures **5** & **S6**). These results are consistent with
506 findings that MPK11 did not enable high CO_2-triggered CBC1 kinase activation *in vitro* and that
507 MPK11 did not interact with HT1 (Takahashi et al., 2022; Jakobson et al., 2016). Furthermore, these
508 data support a hypothesis that MPK12 is diverged from MPK4, which possesses broader functions and
509 a more ubiquitous expression pattern. Therefore, MPK4 can substitute MPK12, but not *vice versa*, when
510 expressed under specific promoters (Figure **5**).

511 **Acknowledgements**

512 This research was supported by Estonian Research Council (Grants PRG430 to H.K., PRG1509 to
513 A.T.G.-S. and PRG757 to I.I.), European Regional Development Fund (Centre of Excellence in
514 Molecular Cell Engineering (CEMCE) to H.K. & Y.-S.W., JST, PRESTO Grant Number JPMJPR21D8
515 to Y.T. and a National Science Foundation grant (MCB-1900567) to J.I.S.

516 **Author contributions**

517 Y.-S.W. and H.K. conceived the study. Y.-S.W., A.T.G.-S and I.I. designed the research. Y.-S. W., C.-
518 Y. Y., Y.T., K.K., K.P., T.A., O.Y., I.I., and A.T.G.-S. conducted the experiments. Y.-S. W., C.-Y. Y.,

Y.T., K.K., K.P., T.A., I.I., J.I.S, A.T.G.-S. and H.K. analyzed the data. Y.-S.W. and H.K. wrote the manuscript. All authors read and approved the manuscript.

References

Berriri, S., Garcia, A. V., dit Frey, N. F., Rozhon, W., Pateyron, S., Leonhardt, N., Montillet, J.-L., Leung, J., Hirt, H., & Colcombet, J. (2012). Constitutively Active Mitogen-Activated Protein Kinase Versions Reveal Functions of Arabidopsis MPK4 in Pathogen Defense Signaling. *The Plant Cell*, *24*(10), 4281–4293. https://doi.org/10.1105/TPC.112.101253

Clough, S. J., & Bent, A. F. (1998). Floral dip: a simplified method for Agrobacterium-mediated transformation of Arabidopsis thaliana. *The Plant Journal*, *16*(6), 735–743. https://doi.org/10.1046/J.1365-313X.1998.00343.X

Emirick, M. A., Lee, T., Starkey, P. J., Mumby, M. C., Resing, K. A., & Ahn, N. G. (2006). The gatekeeper residue controls autoactivation of ERK2 via a pathway of intramolecular connectivity. *Proceedings of the National Academy of Sciences of the United States of America*, *103*(48), 18101–18106. https://doi.org/10.1073/PNAS.0608849103

Foyer, C. H., & Noctor, G. (2020). Redox homeostasis and signaling in a higher-CO_2 world. *Annual Review of Plant Biology*, *71*, 157–182. https://doi.org/10.1146/ANNUREV-ARPLANT-050718-095955

Gookin, T. E., & Assmann, S. M. (2014). Significant reduction of BiFC non-specific assembly facilitates *in planta* assessment of heterotrimeric G-protein interactors. *Plant Journal*, *80*(3), 553–567. https://doi.org/10.1111/tpj.12639

Hall, R. A., De Sordi, L., MacCallum, D. M., Topal, H., Eaton, R., Bloor, J. W., Robinson, G. K., Levin, L. R., Buck, J., Wang, Y., Gow, N. A. R., Steegborn, C., & Mühlschlegel, F. A. (2010). CO_2 acts as a signalling molecule in populations of the fungal pathogen *Candida albicans*. *PLoS Pathogens*, *6*(11). https://doi.org/10.1371/JOURNAL.PPAT.1001193

Hamel, L.-P. P., Nicole, M.-C. C., Sritubtim, S., Morency, M.-J. J., Ellis, M., Ehlting, J., Beaudoin, N., Barbazuk, B., Klessig, D., Lee, J., Martin, G., Mundy, J., Ohashi, Y., Scheel, D., Sheen, J., Xing, T., Zhang, S., Seguin, A., & Ellis, B. E. (2006). Ancient signals: comparative genomics of plant MAPK and MAPKK gene families. *Trends in Plant Science*, *11*(4), 192–198. https://doi.org/10.1016/j.tplants.2006.02.007

Hashimoto-Sugimoto, M., Negi, J., Monda, K., Higaki, T., Isogai, Y., Nakano, T., Hasezawa, S., & Iba, K. (2016). Dominant and recessive mutations in the Raf-like kinase HT1 gene completely disrupt stomatal responses to CO_2 in *Arabidopsis*. *Journal of Experimental Botany*, *67*(11), erw134. https://doi.org/10.1093/jxb/erw134

Hashimoto, M., Negi, J., Young, J., Israelsson, M., Schroeder, J. I., & Iba, K. (2006). *Arabidopsis* HT1 kinase controls stomatal movements in response to CO_2. *Nature Cell Biology*, *8*(4), 391–397. https://doi.org/10.1038/ncb1387

Hiyama, A., Takemiya, A., Munemasa, S., Okuma, E., Sugiyama, N., Tada, Y., Murata, Y., & Shimazaki, K. (2017). Blue light and CO_2 signals converge to regulate light-induced stomatal opening. *Nature Communications*, *8*(1), 1284. https://doi.org/10.1038/s41467-017-01237-5

Hõrak, H., Sierla, M., Tõldsepp, K., Wang, C., Wang, Y.-S., Nuhkat, M., Valk, E., Pechter, P., Merilo, E., Salojärvi, J., Overmyer, K., Loog, M., Brosché, M., Schroeder, J. I., Kangasjärvi, J., & Kollist, H. (2016). A dominant mutation in the HT1 kinase uncovers roles of MAP kinases and GHR1 in CO_2-induced stomatal closure. *The Plant Cell*, *28*(10), 2493–2509. https://doi.org/10.1105/tpc.16.00131

Hu, S., Xie, Z., Onishi, A., Yu, X., Jiang, L., Lin, J., Rho, H. sool, Woodard, C., Wang, H., Jeong, J. S., Long, S., He, X., Wade, H., Blackshaw, S., Qian, J., & Zhu, H. (2009). Profiling the human protein-DNA interactome reveals ERK2 as a transcriptional repressor of interferon signaling. *Cell*, *139*(3), 610–622. https://doi.org/10.1016/j.cell.2009.08.037

Ichimura, K., Shinozaki, K., Tena, G., Sheen, J., Henry, Y., Champion, A., Kreis, M., Zhang, S., Hirt, H., Wilson, C., Heberle-Bors, E., Ellis, B. E., Morris, P. C., Innes, R. W., Ecker, J. R., Scheel, D., Klessig, D. F., Machida, Y., Mundy, J., … Walker, J. C. (2002). Mitogen-activated protein kinase cascades in plants: a new nomenclature. *Trends in Plant Science*, *7*(7), 301–308. https://doi.org/10.1016/S1360-1385(02)02302-6

Jakobson, L., Vaahtera, L., Tõldsepp, K., Nuhkat, M., Wang, C., Wang, Y.-S., Hõrak, H., Valk, E., Pechter, P., Sindarovska, Y., Tang, J., Xiao, C., Xu, Y., Gerst Talas, U., García-Sosa, A. T., Kangasjärvi, S., Maran, U., Remm, M., Roelfsema, M. R. G., … Brosché, M. (2016). Natural variation in *Arabidopsis* Cvi-0 accession reveals an important role of MPK12 in guard cell CO_2 signaling. *PLOS Biology*, *14*(12), e2000322. https://doi.org/10.1371/journal.pbio.2000322

Jammes, F., Song, C., Shin, D., Munemasa, S., Takeda, K., Gu, D., Cho, D., Lee, S., Giordo, R., Sritubtim, S., Leonhardt, N., Ellis, B. E., Murata, Y., & Kwak, J. M. (2009). MAP kinases MPK9 and MPK12 are preferentially expressed in guard cells and positively regulate ROS-mediated ABA signaling. *Proceedings of the National Academy of Sciences of the United States of America*, *106*(48), 20520–20525. https://doi.org/10.1073/PNAS.0907205106/SUPPL_FILE/0907205106SI.PDF

Jumper, J., Evans, R., Pritzel, A., Green, T., Figurnov, M., Ronneberger, O., Tunyasuvunakool, K., Bates, R., Žídek, A., Potapenko, A., Bridgland, A., Meyer, C., Kohl, S. A. A., Ballard,

A. J., Cowie, A., Romera-Paredes, B., Nikolov, S., Jain, R., Adler, J., … Hassabis, D. (2021). Highly accurate protein structure prediction with AlphaFold. *Nature 2021 596:7873*, *596*(7873), 583–589. https://doi.org/10.1038/s41586-021-03819-2

Kollist, T., Moldau, H., Rasulov, B., Oja, V., Rämma, H., Hüve, K., Jaspers, P., Kangasjärvi, J., & Kollist, H. (2007). A novel device detects a rapid ozone-induced transient stomatal closure in intact *Arabidopsis* and its absence in *abi2* mutant. *Physiologia Plantarum*, *129*(4), 796–803. https://doi.org/10.1111/J.1399-3054.2006.00851.X

Kung, J. E., & Jura, N. (2016). Structural basis for the non-catalytic functions of protein kinases. *Structure (London, England: 1993)*, *24*(1), 7. https://doi.org/10.1016/J.STR.2015.10.020

Kushnirov, V. V. (2000). Rapid and reliable protein extraction from yeast. *Yeast.* https://onlinelibrary.wiley.com/doi/epdf/10.1002/1097-0061%2820000630%2916%3A9%3C857%3A%3AAID-YEA561%3E3.0.CO%3B2-B

Lee, J. S., Wang, S., Sritubtim, S., Chen, J. G., & Ellis, B. E. (2009). *Arabidopsis* mitogen-activated protein kinase MPK12 interacts with the MAPK phosphatase IBR5 and regulates auxin signaling. *The Plant Journal*, *57*(6), 975–985. https://doi.org/10.1111/J.1365-313X.2008.03741.X

Mace, P. D., & Murphy, J. M. (2021). There's more to death than life: Noncatalytic functions in kinase and pseudokinase signaling. *The Journal of Biological Chemistry*, *296*. https://doi.org/10.1016/J.JBC.2021.100705

Madhani, H. D., Styles, C. A., & Fink, G. R. (1997). MAP kinases with distinct inhibitory functions impart signaling specificity during yeast differentiation. *Cell*, *91*(5), 673–684. https://doi.org/10.1016/S0092-8674(00)80454-7

Marais, D. L. D., Auchincloss, L. C., Sukamtoh, E., McKay, J. K., Logan, T., Richards, J. H., & Juenger, T. E. (2014). Variation in MPK12 affects water use efficiency in *Arabidopsis* and reveals a pleiotropic link between guard cell size and ABA response. *Proceedings of the National Academy of Sciences of the United States of America*, *111*(7), 2836–2841. https://doi.org/10.1073/PNAS.1321429111

Marten, H., Hyun, T., Gomi, K., Seo, S., Hedrich, R., & Roelfsema, M. R. G. (2008). Silencing of NtMPK4 impairs CO_2-induced stomatal closure, activation of anion channels and cytosolic Ca^{2+} signals in *Nicotiana tabacum* guard cells. *The Plant Journal*, 55, 698-708. https://doi.org/10.1111/j.1365-313X.2008.03542.x

Matallanas, D., Birtwistle, M., Romano, D., Zebisch, A., Rauch, J., Kriegsheim, A. Von, Kolch, W., von Kriegsheim, A., Kolch, W., Kriegsheim, A. Von, Kolch, W., von Kriegsheim, A., &

Kolch, W. (2011). Raf family kinases: Old dogs have learned new tricks. *Genes & Cancer*, *2*(3), 232–260. https://doi.org/10.1177/1947601911407323

Mirdita, M., Schütze, K., Moriwaki, Y., Heo, L., Ovchinnikov, S., & Steinegger, M. (2022). ColabFold: making protein folding accessible to all. *Nature Methods 2022 19:6*, *19*(6), 679–682. https://doi.org/10.1038/s41592-022-01488-1

Mirdita, M., Steinegger, M., Breitwieser, F., Sö Ding, J., & Levy Karin, E. (2021). Fast and sensitive taxonomic assignment to metagenomic contigs. *Bioinformatics*, *37*(18), 3029–3031. https://doi.org/10.1093/BIOINFORMATICS/BTAB184

Patron, N. J., Orzaez, D., Marillonnet, S., Warzecha, H., Matthewman, C., Youles, M., Raitskin, O., Leveau, A., Farré, G., Rogers, C., Smith, A., Hibberd, J., Webb, A. A. R., Locke, J., Schornack, S., Ajioka, J., Baulcombe, D. C., Zipfel, C., Kamoun, S., … Haseloff, J. (2015). Standards for plant synthetic biology: A common syntax for exchange of DNA parts. *New Phytologist*, *208*(1), 13–19. https://doi.org/10.1111/nph.13532

Petersen, M., Brodersen, P., Naested, H., Andreasson, E., Lindhart, U., Johansen, B., Nielsen, H. B., Lacy, M., Austin, M. J., Parker, J. E., Sharma, S. B., Klessig, D. F., Martienssen, R., Mattsson, O., Jensen, A. B., & Mundy, J. (2000). *Arabidopsis* map kinase 4 negatively regulates systemic acquired resistance. *Cell*, *103*(7), 1111–1120. https://doi.org/10.1016/S0092-8674(00)00213-0

Phelan, D. E., Mota, C., Lai, C., Kierans, S. J., & Cummins, E. P. (2021). Carbon dioxide-dependent signal transduction in mammalian systems. *Interface Focus*, *11*(2). https://doi.org/10.1098/RSFS.2020.0033

Shaw, A. S., Kornev, A. P., Hu, J., Ahuja, L. G., & Taylor, S. S. (2014). Kinases and pseudokinases: lessons from RAF. *Molecular and Cellular Biology*, *34*(9), 1538–1546. https://doi.org/10.1128/MCB.00057-14

Shimada, T. L., Shimada, T., & Hara-Nishimura, I. (2010). A rapid and non-destructive screenable marker, FAST, for identifying transformed seeds of *Arabidopsis thaliana*. *Plant Journal*, *61*(3), 519–528. https://doi.org/10.1111/j.1365-313X.2009.04060.x

Sierla, M., Hõrak, H., Overmyer, K., Waszczak, C., Yarmolinsky, D., Maierhofer, T., Vainonen, J. P., Salojärvi, J., Denessiouk, K., Laanemets, K., Tõldsepp, K., Vahisalu, T., Gauthier, A., Puukko, T., Paulin, L., Auvinen, P., Geiger, D., Hedrich, R., Kollist, H., & Kangasjärvi, J. (2018). The receptor-like pseudokinase GHR1 is required for stomatal closure. *Plant Cell*, *30*(11), 2813–2837. https://doi.org/10.1105/tpc.18.00441

Takahashi, Y., Bosmans, K. C., Hsu, P.-K., Paul, K., Seitz, C., Yeh, C.-Y., Wang, Y.-S.,

652 **Yarmolinsky, D., Sierla, M., Vahisalu, T., McCammon, J. A., Kangasjärvi, J., Zhang, L.,**
653 **Kollist, H., Trac, T., & Schroeder, J. I. (2022).** Stomatal CO_2/bicarbonate sensor consists of
654 two interacting protein kinases, Raf-like HT1 and non-kinase-activity requiring MPK12/MPK4.
655 *Science Advances*, *8*(49). https://doi.org/10.1126/SCIADV.ABQ6161

656 **Taylor, S. S., & Kornev, A. P. (2011).** Protein kinases: evolution of dynamic regulatory proteins.
657 *Trends in Biochemical Sciences*, *36*(2), 65–77. https://doi.org/10.1016/J.TIBS.2010.09.006

658 **Tõldsepp, K., Zhang, J., Takahashi, Y., Sindarovska, Y., Hõrak, H., Ceciliato, P. H. O.,**
659 **Koolmeister, K., Wang, Y.-S., Vaahtera, L., Jakobson, L., Yeh, C.-Y., Park, J., Brosche,**
660 **M., Kollist, H., & Schroeder, J. I. (2018).** Mitogen-activated protein kinases MPK4 and
661 MPK12 are key components mediating CO_2-induced stomatal movements. *The Plant Journal*,
662 *96*(5), 1018–1035. https://doi.org/10.1111/tpj.14087

663 **Tsugama, D., Liu, S., & Takano, T. (2011).** A rapid chemical method for lysing *Arabidopsis* cells
664 for protein analysis. *Plant Methods*, *7*(1). https://doi.org/10.1186/1746-4811-7-22

665

666 Supporting information

667 Supplementary methods: Molecular cloning

668 For split-ubiquitin yeast two-hybrid (Y2H) assays, the DUALhunter kit (Dualsystems Biotech) was
669 used for bait and prey construction. The *HT1* coding sequence without a stop codon was cloned between
670 two *Sfi*I sites in the pDHB1 bait vector to allow in-frame fusion with the *Cub-LexA-VP16*. For prey
671 constructs, coding sequences of *MPK12* variants and *MPK11* (At1g01560.2) were fused to *NubG-HA*
672 in the pPR3-N vector. Plasmids of pAI-Alg5 (with a native NubI) and pDL2-Alg5 (with a mutated
673 NubG having I13G substitution to prevent spontaneous reconstitution of split ubiquitin) were used as
674 positive and negative prey controls, respectively (Figure **S1a**).

675 For bimolecular fluorescence complementation (BiFC) assays, two different sets of binary constructs
676 were used. In the ratiometric confocal microscopy-based BiFC experiments, all binary constructs were
677 created by introducing gene of interest (*HT1* and *MPKs*) via ligation-independent cloning into a
678 *35S:YFPn* (amino acids 1-173 of eYFP) or *35S:YFPc* (amino acids 155-239 of eYFP) vector as describe
679 in Hõrak et al., 2016. A *35S:SLAC1-CFP* construct was used as a transformation control and a
680 ratiometric reference marker (Figure **S1b**; Hõrak et al., 2016). For the widefield CO_2-dependent BiFC
681 experiments, a modified split mVenus system with a splitting point at the 210th residue (Gookin &
682 Assmann, 2014) was used to reduce background signals. Binary constructs with dual expression
683 cassettes of the *35S:HT1-NmVen210* (amino acids 1-210 of mVenus) and *35S:MPK-CVen210* (amino
684 acids 211-239 of mVenus) were sequentially assembled by Golden Gate cloning. First, the *35S:HT1-*

685 *NmVen210* cassette was assembled into a destination vector, P19_amilCP/pYSWb1, which contained a
686 *P19* silencing suppressor and an *amilCP* dropout. The *amilCP* dropout was flanked by two outward-
687 oriented *Bsa*I sites to allow replacement of the purple chromoprotein with the desired expression
688 cassette by Golden Gate cloning with a GGAG-CGCT linker according to the common syntax for plants
689 (Patron et al., 2015). After introduction of the *35S:HT1-NmVen210* cassette, another *amilCP* dropout
690 digested with *Sgs*I and *Sal*I was added at the downstream *Mlu*I/*Sal*I site to allow assembly of the
691 *35S:MPK-CVen210* cassette (Figure **S1c**).

692 For *in planta* complementation, four sets of *MPK* cassettes were assembled by Golden Gate cloning in
693 the destination vector, pFAST-R_amilCP/pYSWb1, which contains a *pFAST-R* marker (Shimada et al.,
694 2010) and an *amilCP* dropout for Golden Gate assembly, as well as a *P19* silencing suppressor and a
695 hygromycin-resistance cassette (*HygR*). The first set (*pMPK12:gMPK12_tMPK12*) contained a 2.7 kb
696 genomic sequence of *MPK12* encompassing 543 bp upstream of the start codon (*pMPK12*) and 520 bp
697 downstream of the stop codon (*tMPK12*). The second set (*pMPK12:gMPK12-mVenus-HA_tMPK12*)
698 contained the 2.7 kb genomic *MPK12* fused to a *mVenus-HA* tag. The third set (*pUBQ10:cMPK12-*
699 *mVenus-HA_tNOS*) had a cDNA copy of *MPK12* fused to *mVenus-HA* driven by an *Arabidopsis*
700 *ubiquitin10* promoter (*pUBQ10*) and the *nopaline synthase* terminator (*tNOS*) from *Agrobacterium*
701 *tumefaciens*. Each of the three sets include MPK12 from the wild-type Columbia-0 (Col-0) and four
702 variants with 1 or 2 amino acid substitutions, which were created by overlap-PCR. The fourth set
703 (*pMPK12:cMPK-mVenus-HA_tMPK12*) had a cDNA copy of various MPKs (MPK4, 11, 12 and
704 chimeras/truncations) fused to a *mVenus-HA* tag under the control of *MPK12* regulatory elements
705 (Figure **S4a**).

706 For protein expression in the baculovirus/insect cell system, the HT1 cDNA was fused with a N-
707 terminal His tag (MHHHHHH; 6xHis following a methionine), mCherry and a TEV protease cleavage
708 site. The entire coding sequence was cloned at the *Sal*I/*Bcu*I site of the pFastBac1 vector (Thermo
709 Scientific). Similarly, the MPK12 cDNA was N-terminally fused with a twin strep tag followed by a
710 HA epitope and mVenus (Figure **S1d**).

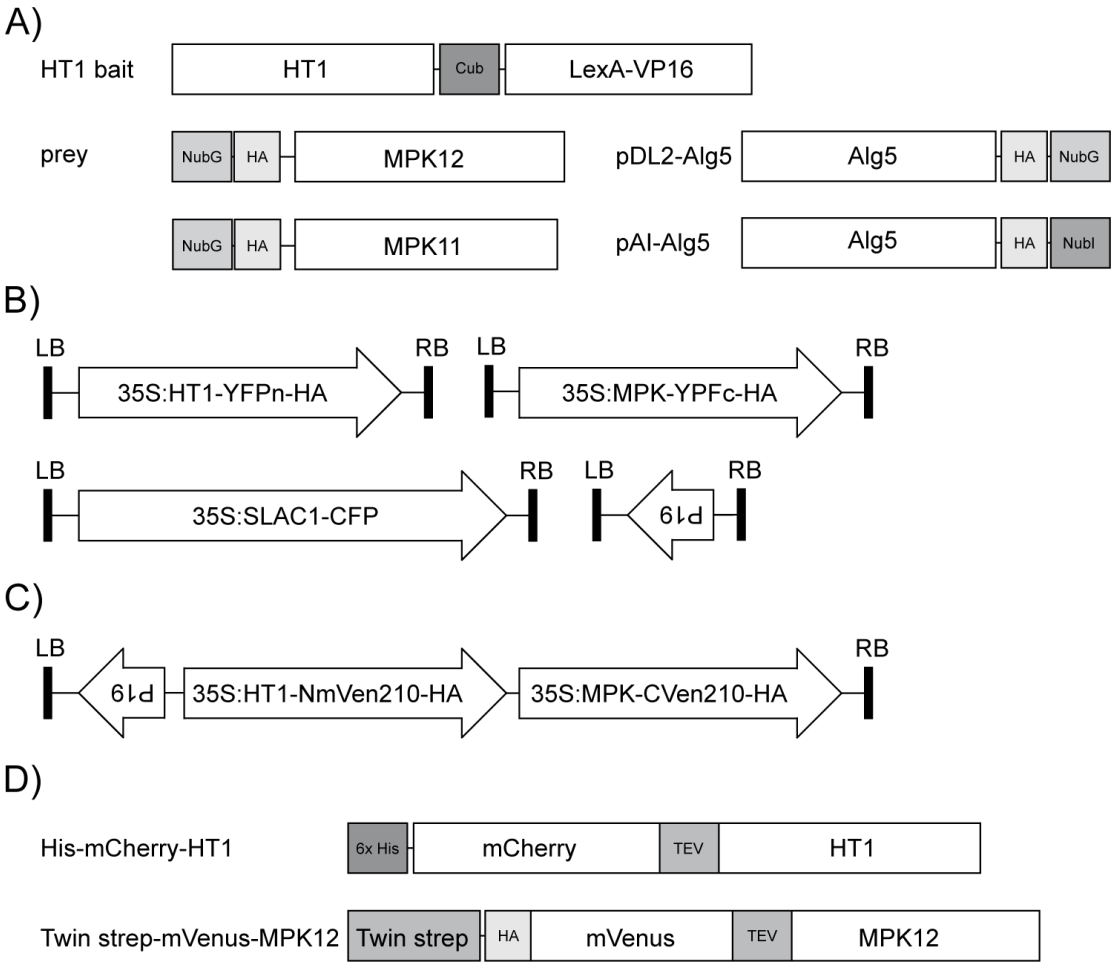

Figure S1. Construct schemes used in this study.

A) Diagram of constructs used in split-ubiquitin Y2H assays: HT1, as a bait, is fused to the C-terminal half of ubiquitin (Cub) and a transcription factor (LexA-VP16); MPK12s and MPK11 are fused to a mutated N-terminal half of ubiquitin with an I13G substitution (NubG) and a hemagglutinin (HA) tag; a yeast Alg5 coding sequence fused to an HA tag and NubG (pDL2-Alg5) is used as a negative prey control, whereas Alg5 fused to HA and the native N-terminal ubiquitin (NubI) is used as a positive control (pAI-Alg5).

B) Diagram of constructs used in ratiometric BiFC assay: the T-DNA region of four separate binary constructs are shown; each contains either a P19 silencing suppressor, a HT1 fused to the N-terminal half (1-173 amino acids) of eYFP and a HA tag (HT1-YFPn-HA), a MPK fused to the C-terminal half (155-239 amino acids) of eYFP and a HA tag (MPK-YFPc-HA), or a plasma membrane-localized Slow Anion Channel 1 (SLAC1) fused to eCFP as a transformation and reference control.

C) Diagram of constructs used in the widefield fluorescence microscopy-based BiFC assay: the T-DNA region contains a P19 suppressor and two split mVenus fusions (split between 210th and 211th amino acids) with a HA tag (HT1-NmVen210-HA & MPK-CVen210-HA) for interaction study; all three cassettes are in one plasmid to ensure coexpression.

D) Diagram of constructs used for recombinant protein expression using the baculovirus/insect cell system. The HT1 construct contains a 6xHis tag immediately following the methionine, as well as a mCherry fluorescent protein and a TEV protease cleavage site, whereas the MPK12 construct has a twin strep tag followed by a HA epitope, mVenus and a TEV site.

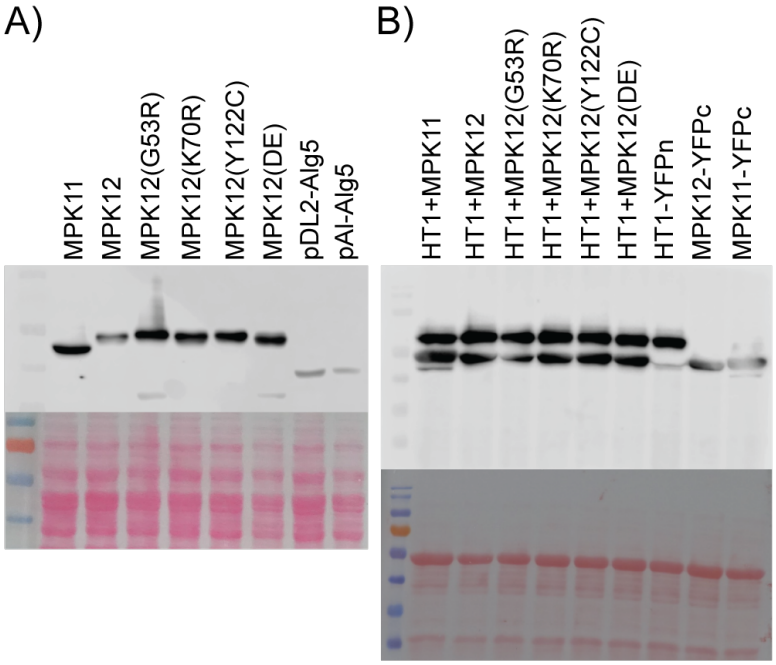

Figure S2. Western blot analyses indicate successful expression of all fusion proteins in the interaction studies.

A) Western blot analyses with anti-HA antibody (upper panels) and Ponceau S staining (lower panels) of proteins extracted from yeast cells in the Y2H study show expression of all HA-fusion proteins from the prey constructs; no signals from HT1 due to lack of a HA tag in the bait construct.

B) Western blot analyses with anti-HA antibody (upper panels) and Ponceau S staining (lower panels) of proteins extracted from *Nicotiana benthamiana* leaves in the ratiometric BiFC experiments show expression of HT1-YFPn and MPK-YFPc proteins; proteins extracted from leaves infiltrated with *SLAC1-CFP* plus *HT1-YFPn*, *MPK12-YFPc* or *MPK11-YFPc* are used as size controls for HT1 and MPK fusions.

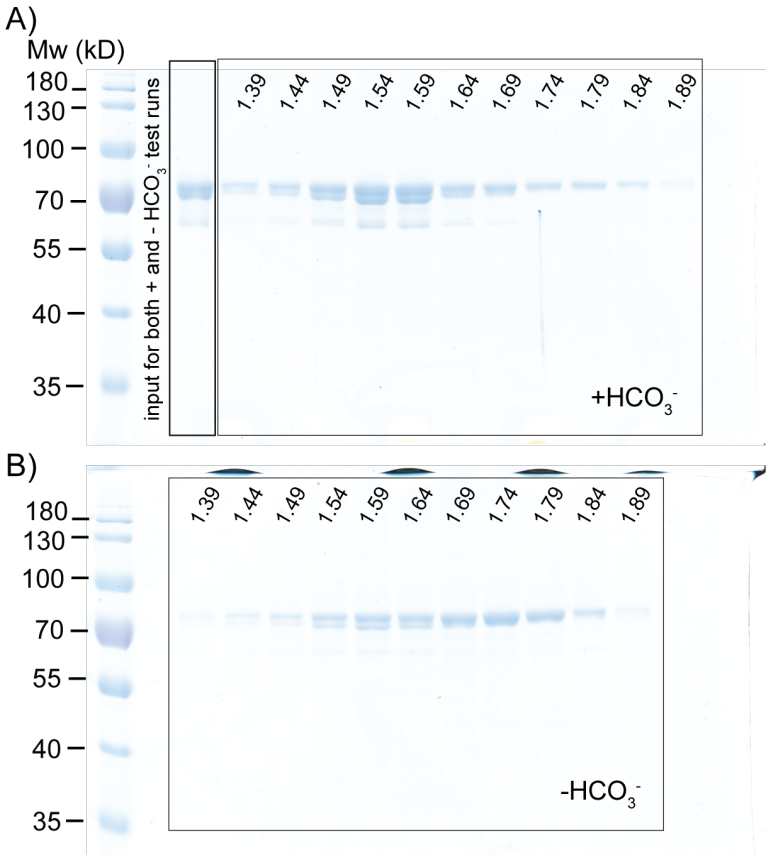

Figure S3. Whole gels of protein fractions shown in Fig. 2e.

Coomassie brilliant blue stained 10% polyacrylamide-SDS gels showing total proteins in the peak fractions of the chromatography runs with HCO_3^- in **a)** and without added HCO_3^- in **b)** as depicted in **Fig. 2e**; the starting elution volumes of the sampled chromatography fractions are indicated on top of each lane; the molecular weight (Mw) standards in these gels are indicated on the left; expected Mw of the His-mCherry-HT1 and twin strep-mVenus-MPK12 proteins are 72.9kD and 74.6kD, respectively.

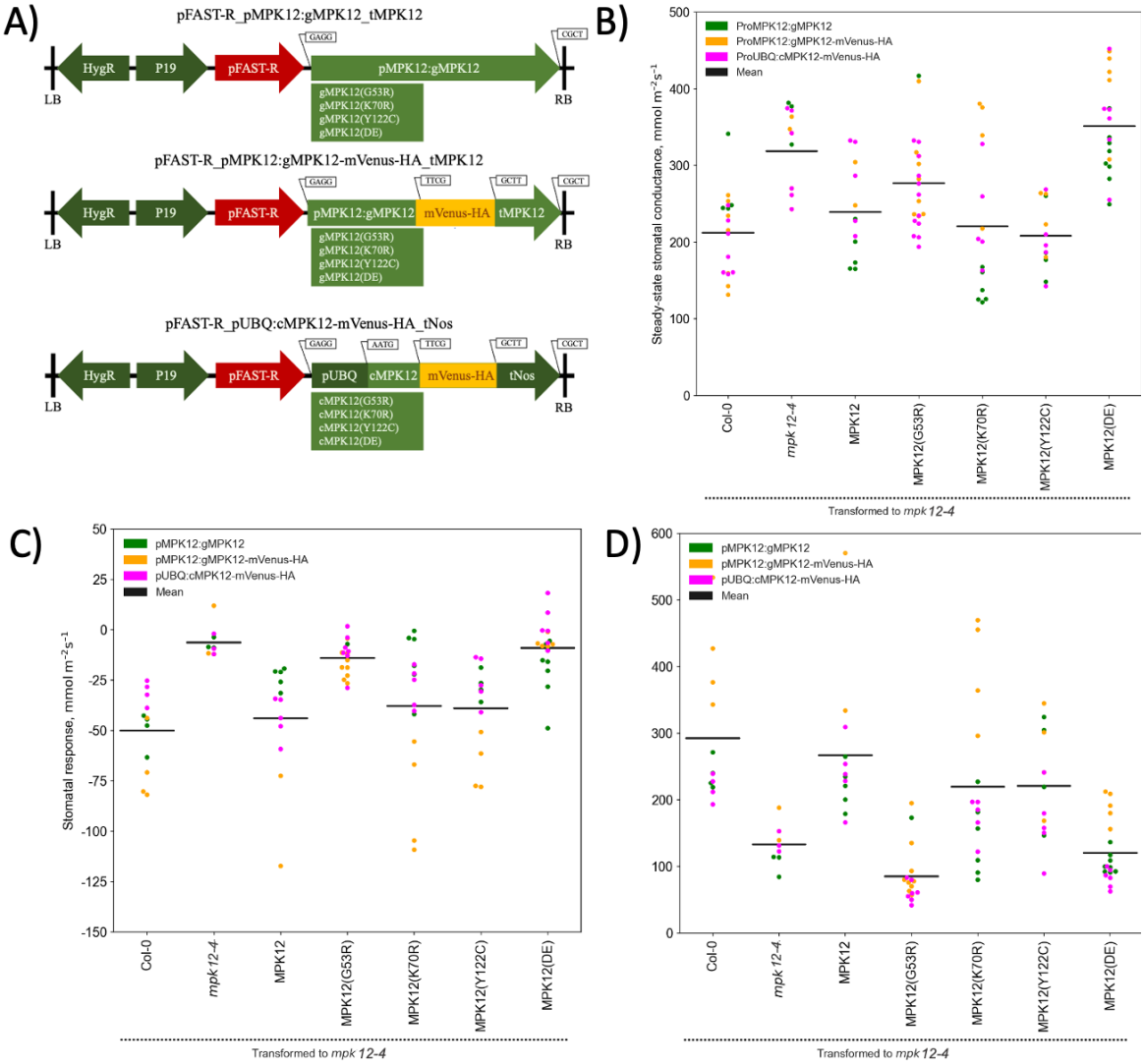

Figure S4. MPK12 variants with K70R and Y122C substitutions, but not the G53R or DE versions, can complement CO_2 responses in the *mpk12-4* plants.

A) Diagrams of binary vectors used to transform *mpk12-4* plants: LB- left border T-DNA sequence; RB- right border T-DNA sequence; HygR- Hygromycin B resistance marker gene; P19 – gene silencing suppressor; pFAST-R - *A. thaliana Oleosin* gene fused with a red fluorescence protein sequence; pMPK12 – *MPK12* promoter; gMPK12 – *MPK12* gene sequence with exons and introns; pUBQ – *A. thaliana ubiquitin 10* promoter; cMPK12 – MPK12 coding sequence without introns; mVenus – a yellow fluorescent protein gene; HA - Human Influenza Hemagglutinin tag; tNos - *A. tumefaciens Nopaline synthase* terminator. The overhangs after *Bsa*I digestion of the Golden Gate parts and the PCR products are depicted above the respective parts.

B) to **D)** Summary of steady state stomatal conductance in **b**), high CO_2 (from 420 ppm to 800 ppm)-induced closure in **c**), and low CO_2 (from 420 ppm to 100 ppm)-induced opening in **d**) in T1 plants. The stomatal response is calculated as a difference between the conductance at ambient CO_2 (420 ppm) before and after 16 minutes of the treatment; dots of different color denote individual T1 plants with binary constructs of the matching color, whereas the black horizontal lines are the average conductance.

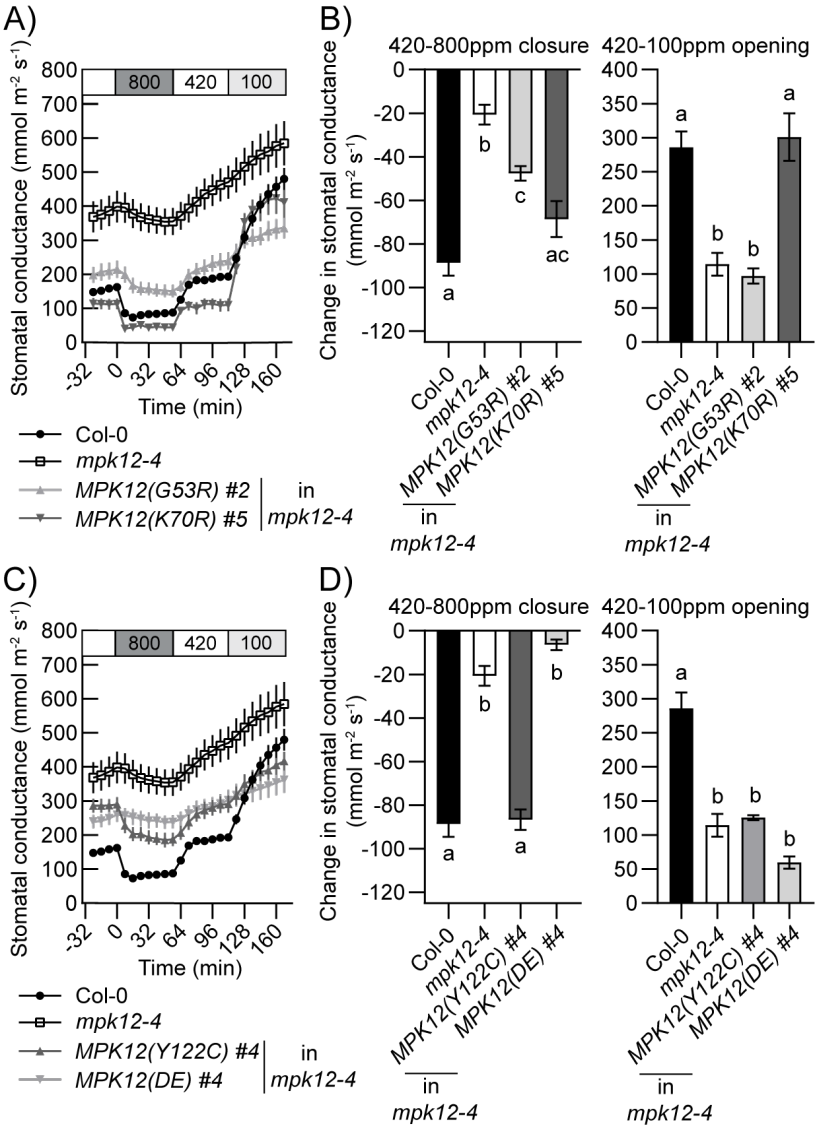

Figure S5. Kinase activity of MPK12 is not required for CO_2 induced stomatal movements. (This data displays same experiments shown in Fig. 3, but using different T2 lines)

A, C) Time-resolved patterns of whole-plant stomatal conductance in response to changes in CO_2 concentrations (in parts per million; ppm) as indicated on top of the panels; intact plants of Col-0 (n=13), *MPK12* deletion line *mpk12-4* (n=12), and *mpk12-4* transformed with *MPK12(G53R)* (n=6), *MPK12(K70R)* (n=5) in **a)** and *MPK12(Y122C)* (n=4), *MPK12(DE)* (n=4) in **c)** were analyzed; data of Col-0 and *mpk12-4* controls are the same as in **Fig. 3a** because they were obtained in the same experimental set.

B, D) Stomatal closure at 16 min after application of 800 ppm CO_2 (left panels) and stomatal opening after application of 100 ppm CO_2 for 56 min (right panels); statistically significant groups are denoted with different letters (ANOVA with Tukey HSD unequal N post hoc test, $P < 0.05$).

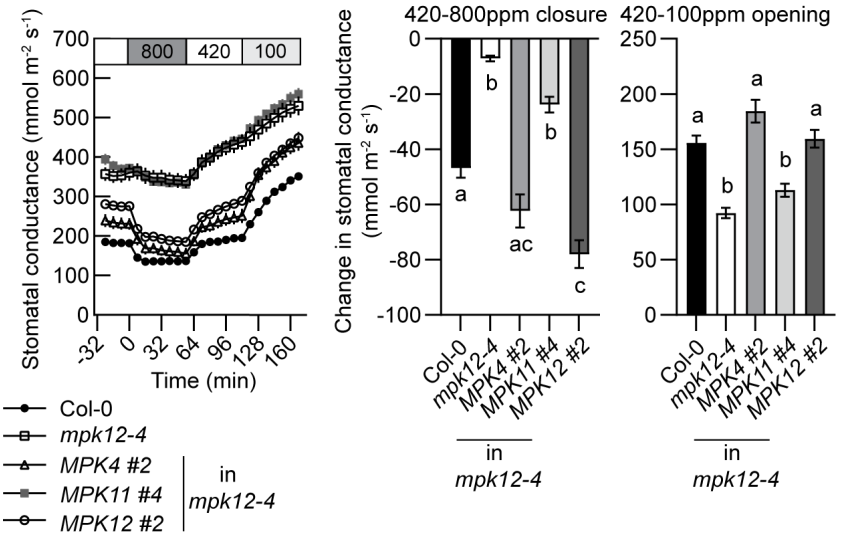

Figure S6. Expression of MPK4 in guard cells can restore *mpk12-4* CO_2 responses but MPK11 cannot. (This data displays the same experiments shown in Fig. 5, but using different T2 lines)

A) Time-resolved patterns of stomatal conductance in response to changes in CO_2 concentrations (in parts per million; ppm) as indicated on top of the panels of Col-0 (n=4), *mpk12-4* (n=4) and *mpk12-4* plants complemented with *pMPK12*:*MPK4* (n=5)/*MPK11* (n=6)/*MPK12* (n=5)-*mVenus-HA* constructs; data of Col-0 and *mpk12-4* controls are the same as in **Fig. 5a** because they were obtained in the same experimental set.

B) Stomatal closure at 16 min after application of 800 ppm CO_2 (left panel) and stomatal opening after application of 100 ppm CO_2 for 56 min (right panel); statistically significant groups are denoted with different letters (ANOVA with Tukey HSD unequal N post hoc test, $P < 0.05$).